1973

Numerical simulation of individual wells in a field simulation model

Ali Mohammed Akbar

NUMERICAL SIMULATION OF INDIVIDUAL WELLS IN A FIELD SIMULATION MODEL

by

ALI MOHAMMED AKBAR, 1941-

A DISSERTATION

Presented to the Faculty of the Graduate School of the

UNIVERSITY OF MISSOURI - ROLLA

In Partial Fulfillment of the Requirements for the Degree

DOCTOR OF PHILOSOPHY

in

PETROLEUM ENGINEERING

1973

M. D. Arnold — Advisor

J. P. Govier

J. C. Wilson

A. Jeter Sandy

R. E. Earlie

G. R. Cuthbertson

ABSTRACT

Conventional numerical simulation of hydrocarbon reservoirs is inadequate for the prediction of bottom-hole pressures at production wells. This problem can be overcome by using a special mathematical model which combines individual well simulation with reservoir simulation. Severe computational instability is commonly encountered in the radial models due to the relatively small grid-blocks and high fluid velocities in the vicinity of the well bore. This instability is found to be more pronounced during depletion of the reservoir when the pressure near the well bore is below bubble-point pressure. A new technique is introduced here for saturation calculations in the critical region near the well. This technique is found to be stable for computing saturations in the small inner elements of the radial grid. Stability is maintained even for the simulation of reservoir behavior within a few inches of the producing sand face.

The mathematical model developed in this study was used to predict performance of a hypothetical oil field, and these predictions were compared to the performance predicted by an areal model. It is suggested that this type of model be used for reservoirs where pressure drawdown

at producing wells is large, and bottom-hole pressure is less than bubble-point pressure.

ACKNOWLEDGMENT

The author wishes to express his sincere appreciation and thanks to his advisor, Dr. M. D. Arnold, for his valuable assistance and selfless guidance, and who so freely contributed his valuable time and knowledge throughout the investigation of this research.

The author is also grateful to Dr. A. H. Harvey for his advice and able guidance in writing this work. He also wishes to thank Professor J. P. Govier and Dr. R. E. Carlile for serving on his committee, and Dr. G. R. Cuthbertson for serving on his committee and serving as the third reader.

Grateful appreciation is also extended to the Kuwait University for financial support of this work.

The author is greatly indebted to his wife, Amira Al-Saigh, and his parents for their encouragement and enduring patience.

TABLE OF CONTENTS

Table of Contents (continued) Page

LIST OF ILLUSTRATIONS

List of Illustrations (continued) Page

LIST OF TABLES

I. INTRODUCTION

Pressures and fluid saturations in a hydrocarbon reservoir may be described at any point by differential equations involving reservoir rock and fluid properties. Numerical simulation of field performance is accomplished by establishing a reference grid, writing appropriate equations for each mesh point, then solving the system of equations by a finite difference technique. Since the number of mesh points must be finite, there is a necessary assumption that each mesh point is representative of a finite segment of the reservoir. Actually, however, pressures are not equal throughout such a segment of a producing field. This inability of a model to predict pressure variations within an element of the reference grid may create problems when the element contains a production or injection well. Since the field simulation model yields a calculated pressure which is representative of the entire element, this pressure is not the bottom-hole pressure of the well. This situation will exist even though the well location may coincide with the grid point which represents the element.

This inability of the model to describe variations within small segments of the reservoir is not unique to the pressure calculation. Fluid saturations computed for a mesh point represent average saturations of a finite segment of the reservoir. Fluid produced from the area of the well bore is handled mathematically as if it were withdrawn from the entire area associated with a mesh point. Since the conventional finite difference technique does not adequately describe reservoir conditions near a well, special mathematical techniques are required to handle this problem.

In this study an approach to the calculation of well performances is described. A conventional radial coordinate well simulator was first incorporated within a two-dimensional, three-phase, Cartesian coordinate reservoir simulation model for those areal blocks that contained wells. These two models were joined mathematically by summing the fluxes into the four vertical faces of the grid block in the areal model, and considering the total flux for each phase as influx into the outer annular ring of the radial well simulator.

This approach was found to be adequate above bubble-point pressure. However, problems arose with respect to gas balance when well pressure declined below the bubble point and free gas appeared near the well bore. For this situation, the gas-oil ratio calculated from the radial model at the innermost cell was higher than that calculated from the corresponding

areal block. This situation arose because the radial grid elements near the well bore were drawn down below bubble-point pressure, while the average pressure both in the radial model and in the corresponding areal model block was still above saturation pressure. This condition created instability in the radial model material balance calculation for grid elements near the well bore, where the pressure gradients were high and the elements were small.

In order to eliminate this instability, a modified technique for calculating saturations near the well bore was developed. The purpose of this new technique was to improve the material balance sufficiently to avoid the prediction of excessive gas production by the radial simulation model. It is shown later in this work that the new technique will theoretically achieve a perfect material balance. However, machine round-off errors and the use of estimated implicit coefficients prevent the attainment of this ideal.

The method of simulation which was developed was tested using data from a hypothetical petroleum reservoir under natural depletion drive. The results of this study are discussed in a later section.

II. LITERATURE REVIEW

A mathematical petroleum reservoir simulation model may be used to represent the behavior of individual wells or complex petroleum reservoir-aquifer systems.[1,2,3] Several methods have been employed for predicting well bottom-hole pressures from the results computed by numerical reservoir simulators. Mesh point pressures computed by these simulators have been used to a limited extent as bottom-hole pressures.[4] However, this technique has always been considered inadequate because of the known lack of resolution in areal models. A somewhat more useful technique is to reduce permeability at mesh points corresponding to producing wells so that computed pressures equal measured bottom-hole pressures. This method can be expected to give consistent results only when a single fluid phase is flowing.

Another method which has been suggested is that pressure distribution be represented by means of piecewise-polynomial approximations.[5] The technique involves the use of high order polynomials to represent the immediate vicinity of the well bore, and lower order polynomials to represent points more remote from the well.

Another procedure which has been used with some success is the estimation of bottom-hole pressure by extrapolation of pressures from grid blocks adjacent to the block in which the well is located. The extrapolation is calculated by Darcy's law written in radial form and integrated for steady-state conditions. Although the technique is satisfactory for some applications, it can lead to erroneous results for some cases. For example, the method does not give correct results when pressure immediately adjacent to the well bore is drawn down below the bubble point. This condition may generate a gas saturation in the vicinity of the bore hole which is not accounted for by the extrapolation. Since the increase in gas saturation reduces relative permeability to oil, a bottom-hole pressure that is too high will be predicted.

van Poolen, Breitenbach, and Thurneau[6] developed a method for comparing pressures calculated by a numerical simulation model with observed field pressures. The technique used a pressure build-up curve obtained from field measurements to locate the point in the reservoir which grid pressure in the model actually represents.

Individual well simulation has been discussed by several investigators. This type of simulation employs a radial model for the specific purpose of studying water or gas coning problems. Such a model simulates only that portion of the reservoir associated with a single well,

and it does not integrate the well simulation model with the field model. Coning models are inherently less stable than areal models, and this problem of stability has been discussed by several authors.

Welge and Weber[7] presented a paper on water coning which recognized the limitation of explicit coefficients. In order to overcome the problem, these authors applied an arbitrary limitation on the maximum saturation change during a time step. While this method is workable for certain classes of problems, it is not rigorous and is not generally applicable. The severe computational instability which is commonly encountered in the simulation of coning is due to the combinations of high fluid velocities and small pore volumes in grid elements near the well bore. Blair and Weinaug[8] further explored the problems resulting from explicitly determined coefficients and formulated a coning model which used implicit coefficients and mobilities obtained by an iterative procedure. This technique resulted in a significant improvement in stability. McDonald and Coats,[9] and Letkman and Ridings[10] verified the Blair and Weinaug technique and reported a new method for calculating saturations which utilizes fully implicit equations. They also emphasized the need for including implicit mobilities in the production term. These investigators showed that better stability and convergence could be obtained by this fully implicit method.

There have been two papers presented which examine detailed

behavior of individual wells in a multi-well reservoir simulation model. Mrosovsky and Ridings[11] presented a theoretical approach which used a two-dimensional, radial well simulator within a three-dimensional reservoir simulation model. Akbar, Arnold, and Harvey[12] presented a technique for computing bottom-hole pressure by incorporating a one-dimensional radial well simulator into a two-dimensional areal reservoir simulation model. The present research work is an extension of this study.

III. DEVELOPMENT OF THE MODELS

A general discussion of the criteria used for developing the conventional areal and radial models used in this study is presented in this chapter. Detailed development and derivations have been relegated to the appendices. This chapter includes discussion of the mathematical basis for development, the boundary conditions, the production and injection terms, and the methods of solution.

A. Mathematical Description of the Models

Both the areal and the radial models are three-phase numerical simulators. The mathematics developed accounts for effects of capillary forces between the oil and water phases, reservoir heterogeneity, and rock and fluid compressibilities.

1. Areal Reservoir Model

The areal model used in this study is a two-dimensional simulator which accounts for effects of gravity, anisotropy, and structural dip in addition to those effects mentioned earlier which are applicable to both models. As illustrated in Figure 1, the grid system which was used provides for variable spacing. The development of the mathematical basis for calculating pressures and

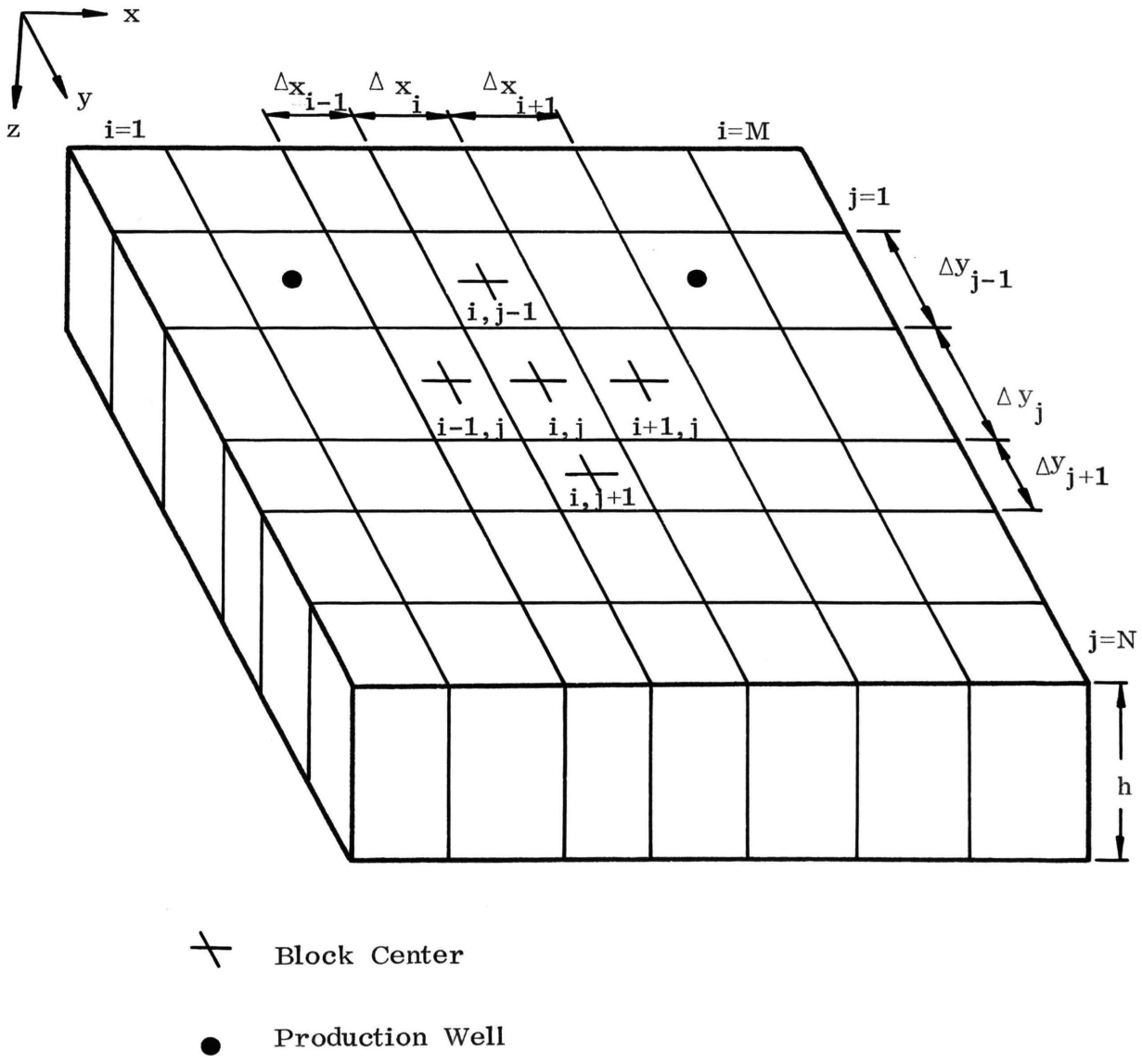

Figure 1. Grid Pattern for the Areal Simulation Model

saturations for this model follows.

Pressure Computation. The pressure calculations in the areal model are made by solving a finite difference equation based on the partial differential equation which is derived in Appendix B-1.

$$(\beta_o - \beta_g R_s)\ \nabla \cdot (\lambda_o \nabla \Phi_o) + \beta_w\ \nabla \cdot (\lambda_w \nabla \Phi_w)$$

$$+ \beta_g\ \nabla \cdot (\lambda_g \nabla \Phi_g) + \beta_g\ \nabla \cdot (\lambda_o R_s \nabla \Phi_o) - QTERM$$

$$= h\ \phi\ (C_r + C_w S_w - \frac{S_o}{\beta_o}\ \beta_o' - \frac{S_g}{\beta_g}\ \beta_g' + \frac{\beta_g S_o}{\beta_o}\ R_s')\frac{\partial p}{\partial t} \quad \ldots\ldots\ldots (1)*$$

An implicit finite difference approximation to Equation (1) is:

$$(\beta_o - \beta_g R_s)^{n+1}_{i,j} (\Delta_x T_o \Delta_x \Phi_o)^{n+1}_{i,j} + \beta^{n+1}_{w_{i,j}} (\Delta_x T_w \Delta_x \Phi_w)^{n+1}_{i,j}$$

$$+ \beta^{n+1}_{g_{i,j}} (\Delta_x T_g \Delta_x \Phi_g)^{n+1}_{i,j} + \beta^{n+1}_{g_{i,j}} (\Delta_x T_o R_s \Delta_x \Phi_o)^{n+1}_{i,j}$$

$$+ (\beta_o - \beta_g R_s)^{n+1}_{i,j} (\Delta_y T_o \Delta_y \Phi_o)^{n+1}_{i,j} + (\Delta_y T_w \Delta_y \Phi_w)^{n+1}_{i,j} \beta^{n+1}_{w_{i,j}}$$

$$+ \beta^{n+1}_{g_{i,j}} (\Delta_y T_g \Delta_y \Phi_g)^{n+1}_{i,j} + \beta^{n+1}_{g_{i,j}} (\Delta_y T_o R_s \Delta_y \Phi_o)^{n+1}_{i,j}$$

---

* All symbols are defined in Nomenclature.

$$- QTERM_{i,j}^{n+1} = TRM_{i,j}^{n+1} \Delta_t P \quad \ldots\ldots (2)$$

Rearranging Equation (2) yields the following set of equations:

$$AX_{i,j}^{n+1} P_{i-1,j}^{n+1} + (BX_{i,j}^{n+1} + BY_{i,j}^{n+1} - TRM_{i,j}^{n+1}) P_{i,j}^{n+1}$$

$$+ CX_{i,j}^{n+1} P_{i+1,j}^{n+1} + AY_{i,j}^{n+1} P_{i,j-1}^{n+1} + CY_{i,j} P_{i,j+1}^{n+1}$$

$$= E_{i,j}^{n+1} - TRM_{i,j}^{n+1} P_{i,j}^{n} \quad \ldots\ldots (3)$$

$$i = 1, 2, \ldots, M$$

$$j = 1, 2, \ldots, N$$

The coefficients appearing in Equation (3) are defined in Appendix B-2. Derivations of Equations (2) and (3) are presented in Appendix B-2.

Equation (3) is written about each point in the two-dimensional reference grid. Thus a total of (MxN) equations are obtained. Application of appropriate boundary conditions reduces the number of unknown quantitites to (MxN). In matrix notations, the resulting set of equations may be written

$$A\overline{P} = \overline{D} \quad \ldots\ldots (4)$$

where $\overline{P}$ is the solution vector, $\overline{D}$ is the vector of known parameters,

and A is an $(MxN)^2$ penta-diagonal matrix of coefficients. Since the implicit coefficients are known, the system may be solved as a set of linear equations. The techniques used are discussed in a later section of this chapter.

Saturation Computation. Each phase saturation in the areal model is calculated separately and explicitly using its respective flow equation. These equations are derived in Appendix B-4, and are written for oil, water, and gas respectively, as follows:

$$S_{o_{i,j}}^{n+1} = (AMOX_{i,j}^{n+1} + AMOY_{i,j}^{n+1} - QOT_{i,j}^{n+1} + S_{o_{i,j}}^{n})/COMPRO_{i,j}^{n+1} \quad \ldots\ldots (5)$$

$$S_{w_{i,j}}^{n+1} = (AMWX_{i,j}^{n+1} + AMWY_{i,j}^{n+1} - QWT_{i,j}^{n+1} + S_{w_{i,j}}^{n})/COMPRW_{i,j}^{n+1} \quad \ldots. (6)$$

$$S_{g_{i,j}}^{n+1} = (AMGX_{i,j}^{n+1} + AMGY_{i,j}^{n+1} + AMSGX_{i,j}^{n+1} + AMSGY_{i,j}^{n+1}$$

$$- QGT_{i,j}^{n+1} - RST_{i,j}^{n+1} + S_{g_{i,j}}^{n})/COMPRG_{i,j}^{n+1} \quad \ldots\ldots\ldots\ldots\ldots (7)$$

The terms in Equations (5), (6), and (7) are derived and defined in Appendix B-4. The saturations are calculated sequentially after the pressures and the terms containing implicit potential gradients. There are (MxN) equations which must be solved. However, each equation

contains only one unknown quantity, and the calculations are explicit in nature even though the coefficients appear as implicit quantities. This computation is discussed in a later section of this chapter.

2. Radial Model Well Simulator

The well simulator is a one-dimensional, three-phase, radial coordinate model. The grid system used is shown in Figure 2. One of these models is assigned to each of those wells which has been selected for detailed analysis.

Pressure Computation. The unsteady-state radial model flow equation (which is derived in Appendix C-1) may be written as follows:

$$\frac{1}{r}(\beta_o - \beta_g R_s)\frac{\partial}{\partial r}\left(r\,\lambda_{o_r}\frac{\partial \Phi_o}{\partial r}\right) + \frac{1}{r}\beta_w\frac{\partial}{\partial r}\left(r\,\lambda_{w_r}\frac{\partial \Phi_w}{\partial r}\right)$$

$$+ \frac{1}{r}\beta_g\frac{\partial}{\partial r}\left(r\,\lambda_{g_r}\frac{\partial \Phi_g}{\partial r}\right) + \frac{1}{r}\beta_g\frac{\partial}{\partial r}\left(r\,\lambda_{o_r}R_s\frac{\partial \Phi_o}{\partial r}\right) - \text{QTERM}$$

$$= \phi\left(C_r + S_w C_w - \frac{S_o}{\beta_o}\beta_o' - \frac{S_g}{\beta_g}\beta_g' + \frac{\beta_g S_o}{\beta_o}R_s'\right)\frac{\partial P}{\partial t} \qquad (8)$$

An implicit difference approximation to Equation (8) is

$$\frac{1}{r}\left[(\beta_o - \beta_g R_s)_i^{n+1}\left(\Delta_r T_{o_r}\Delta_r \Phi_o\right)_i^{n+1} + \beta_{w_i}^{n+1}\left(\Delta_r T_{w_r}\Delta_r \Phi_w\right)_i^{n+1}\right.$$

$$\beta_{g_i}^{n+1} (\Delta_r T_{g_r} \Delta_r \Phi_g)_i^{n+1} + \beta_{g_i}^{n+1} (\Delta_r T_{o_r} R_s \Delta_r \Phi_o)^{n+1}]$$

$$- QTERM_i^{n+1} = TR_i^{n+1} \Delta_t P \quad \ldots\ldots\ldots\ldots\ldots\ldots\ldots\ldots\ldots\ldots\ldots\ldots (9)$$

Rearranging Equation (9) yields the following:

$$AR_i^{n+1} P_{i-1}^{n+1} + BR_i^{n+1} P_i^{n+1} + CR_i^{n+1} P_{i+1}^{n+1} = D_i^{n+1} \quad \ldots\ldots\ldots\ldots\ldots (10)$$

$$i = 1, 2, \ldots, I.$$

The coefficients of Equation (9) are derived in Appendix C-2. This equation is written for each of the radial grid blocks which comprise the radial well simulator. Thus a total of I equations are obtained. Application of appropriate boundary conditions reduces the number of unknown quantities to I. In matrix notation, the resulting set of equations may be written

$$A\overline{P} = \overline{D} \quad \ldots\ldots\ldots\ldots\ldots\ldots\ldots\ldots\ldots\ldots\ldots\ldots\ldots\ldots\ldots\ldots\ldots\ldots\ldots\ldots\ldots\ldots (11)$$

where $\overline{P}$ is the solution vector, $\overline{D}$ is the vector of known parameters, and A is an (IxI) tri-diagonal matrix of coefficients. It is assumed that the implicit coefficients are known; therefore, the system can be solved as a set of linear equations. The solution of Equation (11) is discussed later in this chapter.

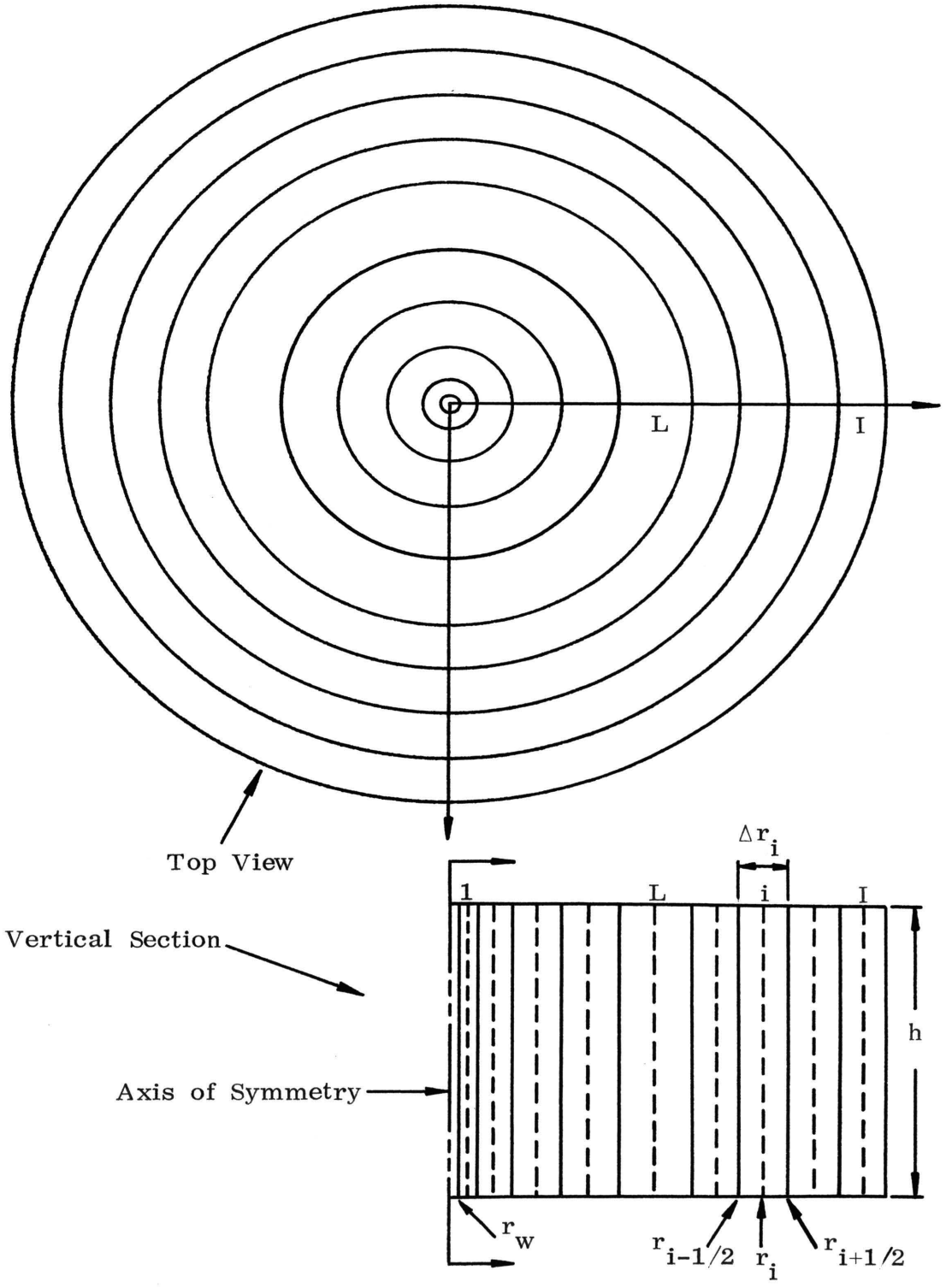

Figure 2. Grid Pattern for the Well Simulation Models

Saturation Computation. Each phase saturation in the radial model is calculated by relationships similar to Equations (5), (6), and (7) written in radial form. This type of calculation is used for radial cells from L+1 to I as shown in Figure 2. A modified saturation computation is used for radial cells 1 to L. This is the region of instability in the standard radial model. This method is a new approach to the stability problem and is discussed in detail in a later chapter.

B. Boundary Conditions

Closed boundaries are assumed for the areal simulator. These boundary conditions are satisfied by setting the potential gradients at the boundaries equal to zero. As illustrated by Figure 3, this condition is represented by setting the value of potential in an adjacent dummy block equal to the value of potential in the adjoining boundary block. The "no-flow" boundary requirement is satisfied by assuming that each dummy block has the same dimensions and the same rock and fluid properties as the adjacent grid block. Substitution of these conditions into Equation (3) yields the following values for the coefficients AX, CX, AY and CY at the boundaries:

$$AX_{1,j} = CX_{M,j} = 0 \qquad j = 1, 2, \ldots, N$$

$$AY_{i,1} = CY_{i,N} = 0 \qquad i = 1, 2, \ldots, M.$$

This method of specifying boundary conditions is a standard approach

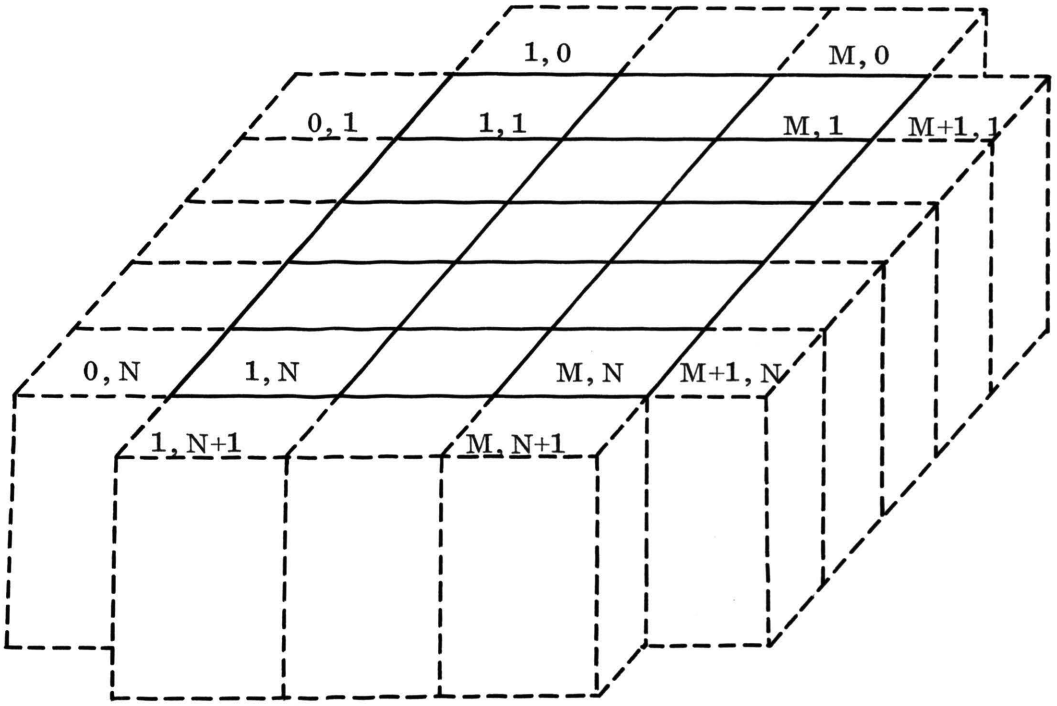

Figure 3. Boundary Elements of the Areal Model

which is used in most reservoir simulators.

Closed boundaries are assumed for the radial well simulator, and the principle described above is applied in the same way as for the areal simulation model. Figure 4 illustrates the grid arrangements used for the radial model. These boundary conditions cause the coefficients AR_1 and CR_I in Equation (10) to vanish. The resulting matrix equation has I unknowns and I equations.

The closed boundaries which have been assumed may appear incompatible with the fluxes shown crossing the boundaries in Figure 4. However, these fluxes are included as injection or production terms. This approach, which combines injection and production terms with closed boundaries, is mathematically identical to the open boundaries shown in Figure 4. This approach is used with the radial well simulator and is discussed in the following section of this chapter.

C. Production and Injection Terms

The total production rates for each component in the areal and radial models must be equal. This is part of the validation criteria discussed in Chapter V. However, it should be noted that since the models are linked mathematically, the production rates calculated for the radial model well simulator are also used in the areal simulation model.

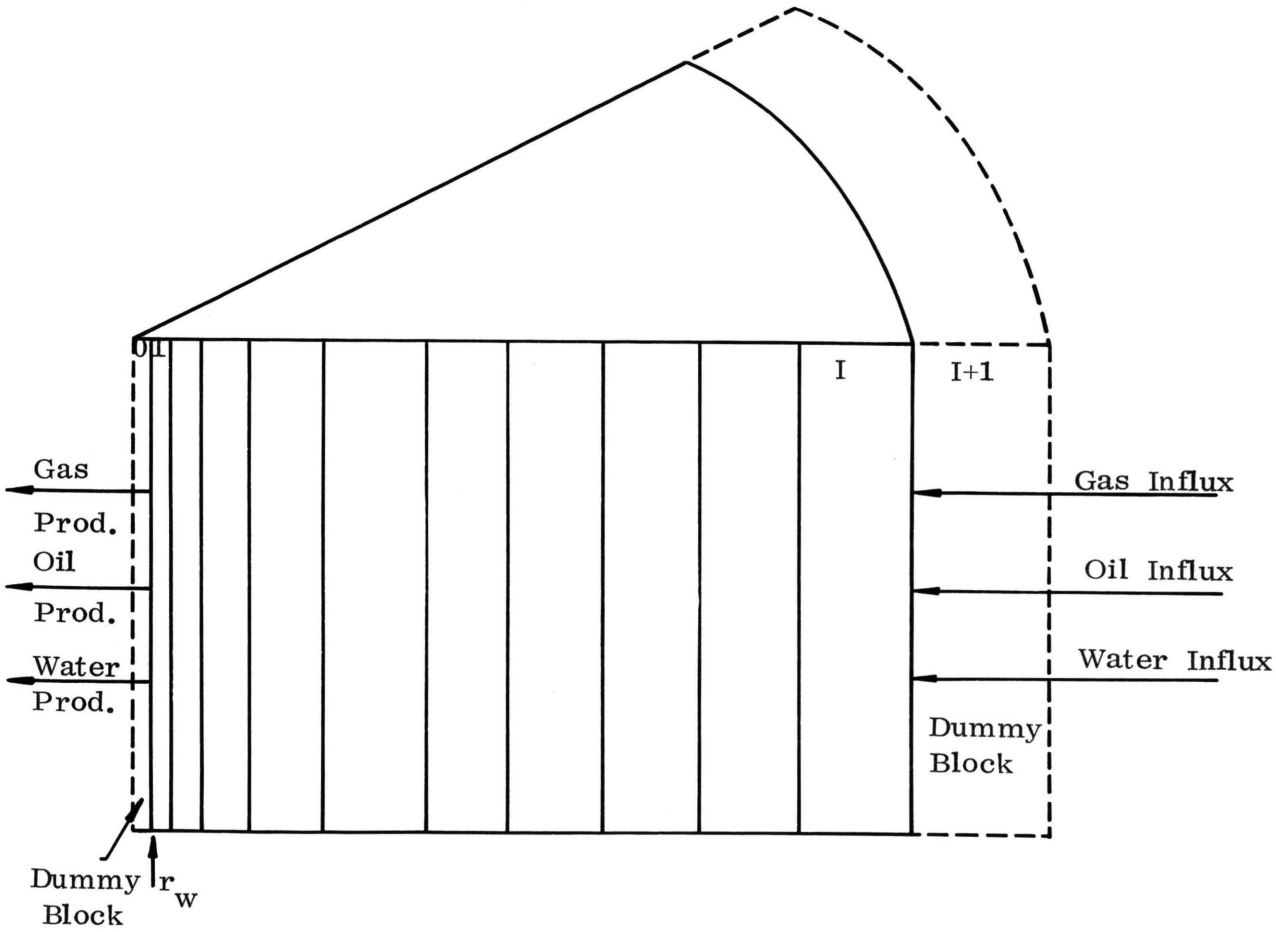

Figure 4. Boundary Elements of the Well Simulator

The combined production term (QTERM), as defined in Appendix B-2, and Appendix C-2 may be different in the radial and areal models, even though the total rates including solution gas are the same. This situation can occur because pressures and solution gas content may be different for the simulators. The actual production terms used are derived in Appendix B-1 and Appendix B-2, respectively, for the areal and radial models. These terms contain rates of production for all mobile phases. In accordance with the convention defined in deriving the equations, fluid production has been considered to be positive in algebraic sign, and fluid injection has been considered negative.

In the simulation of an actual reservoir, oil production rates would be determined primarily by field operating conditions. In this study a constant oil production rate was specified and pressure at the sand face was calculated based on

$$P_{sf} = P_1 - \frac{q_o \beta_o \mu_o \ln(\frac{r_1}{r_w})}{2\pi (KhK_{r_o})_1} \quad \ldots\ldots\ldots\ldots\ldots\ldots\ldots\ldots\ldots\ldots\ldots\ldots (12)$$

where P_{sf} is sand face pressure,

and the productivity index was calculated using the equation

$$PI = \frac{q_o}{P_1 - P_{sf}} = \frac{2\pi (KhK_{r_o})_1}{\beta_o \mu_o \ln(\frac{r_1}{r_w})} \quad \ldots\ldots\ldots\ldots\ldots\ldots\ldots\ldots\ldots\ldots\ldots\ldots (13)$$

The oil production rate remained constant until P_{sf} reached a minimum pressure. Thereafter, P_{sf} was held constant and the well produced at capacity according to

$$q_o = PI(P_1 - P_m) = \frac{2\pi(KhK_{r_o})_1}{\beta_o \mu_o \ln(\frac{r_1}{r_w})} (P_1 - P_m) \quad \ldots\ldots\ldots\ldots\ldots (14)$$

where P_m is a minimum pressure. The total gas production rate was calculated in this study from the oil rate, the mobility ratio of gas to oil, and the solution gas content at the innermost cell of the radial simulator. The production term used in the models contains only free gas rate. Therefore, radial free gas production was adjusted for the areal simulator in such a way that total gas production rate will be the same from both models; this adjustment is necessary to satisfy the Law of Mass Conservation. The adjustment was made by the following equation:

$$q_{g_{i,j}} = (q_{g_1})_R - [(R_{s_{i,j}})_A - (R_{s_1})_R] \, q_{o_{i,j}} \quad \ldots\ldots\ldots\ldots (15)$$

Water production rates were calculated from the oil production rate and the water-oil mobility ratio. No adjustment to equalize water production in the two models was required, since water breakthrough did not occur during the study. According to the theory which has been developed, water production predicted by the two models should be equal.

For production wells, the production term in the radial model was obtained by summing the fluxes for each phase at each of the four

vertical faces of the areal block which includes the well. This scheme is illustrated by Figure 5. These fluxes were used to calculate the overall flux term in the radial model which was applied at the outer annular ring as illustrated by Figure 4. The only adjustment necessary for these fluxes between models was a change of sign. The fluxes from the areal faces are positive for a producing well and were changed to negative quantities to indicate injection into the radial model. No further adjustments were required, since these fluxes were carried as mass rates rather than volumetric rates.

D. Solution of the Numerical Simulators

Equation (3) represents a set of simultaneous equations where pressure at each point is unknown. Several methods were investigated to determine convergence rate and stability. A method which was found to converge rapidly even for highly heterogeneous reservoir conditions was the combination of ADI[13] and pressure residual relaxation method,[14] as illustrated in Appendix B-3. Fluid and rock properties used in the coefficients of Equation (3) were calculated at the new time level t^{n+1} based on a linear extrapolation technique.[15] Each phase saturation in the areal model was calculated using Equations (5), (6), and (7) explicitly.

Equation (10) is the pressure equation for the radial well simulator, and Equation (11) is the matrix notation for Equation (10). The coefficient

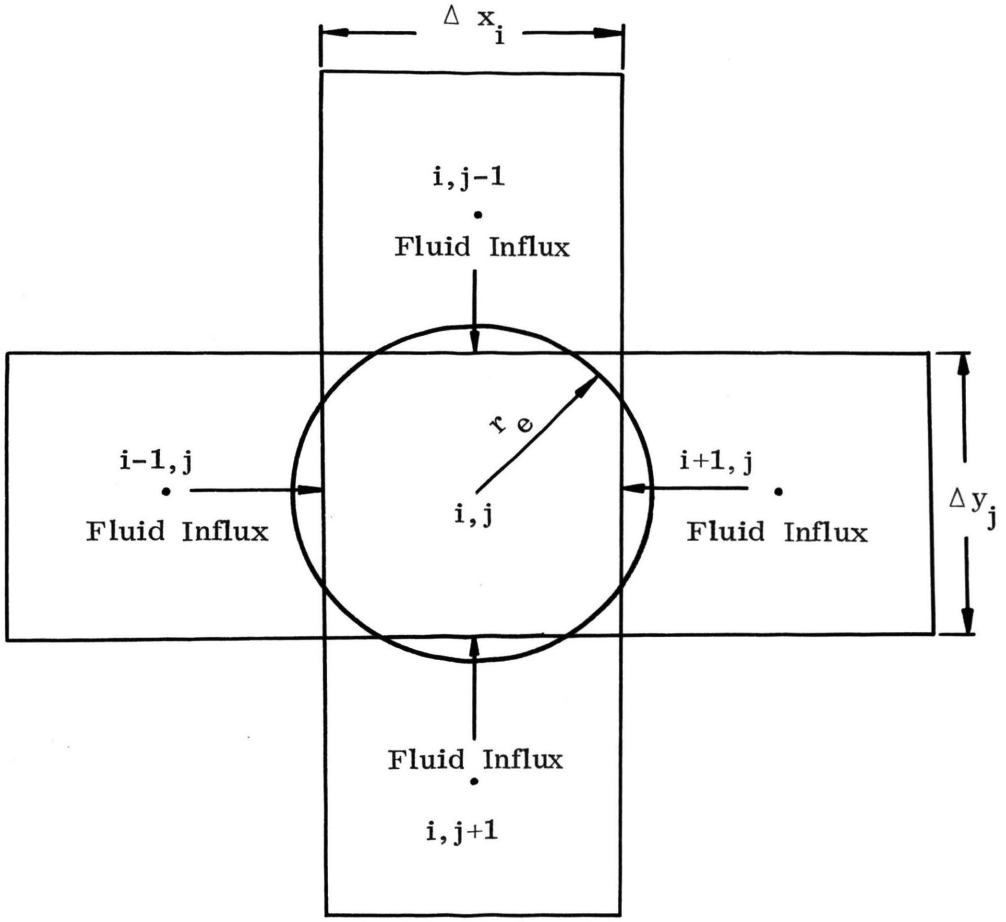

Figure 5. Relation of the Well Simulator to the Areal Simulation Model

matrix A is tri-diagonal in form; it was solved for pressure by Gaussian elimination. Rock and fluid properties used in forming the matrix coefficients A were evaluated at the new time level t^{n+1} by linear extrapolation. Each phase saturation for each radial cell from L+1 through I was calculated using equations similar to Equations (5), (6), and (7), but written in radial form.

IV. NEW TECHNIQUE FOR SATURATION CALCULATION (DYNAMIC APPROACH)

The method presented here for calculating saturations was used in the small annular rings of the radial model which are near the well bore. The technique avoided the stability problems usually encountered in radial simulation models. A standard radial model was used for pressure calculations. These computations were also stable, since the technique used avoided material balance errors which cause instability in the pressure calculations.

The technique for calculating saturations employed a one-dimensional, three-phase radial coordinate simulation model. It assumed unsteady-state flow conditions and accounted for the effects of rock and fluid compressibilities as well as relative permeability. The equations presented later in this chapter were used for the saturation computations; their derivations are presented in Appendix D. The geometric configuration of the simulation grid is illustrated by Figure 6.

The fundamental concept on which the saturation calculation was based is that material balance must be maintained. A derivation of the

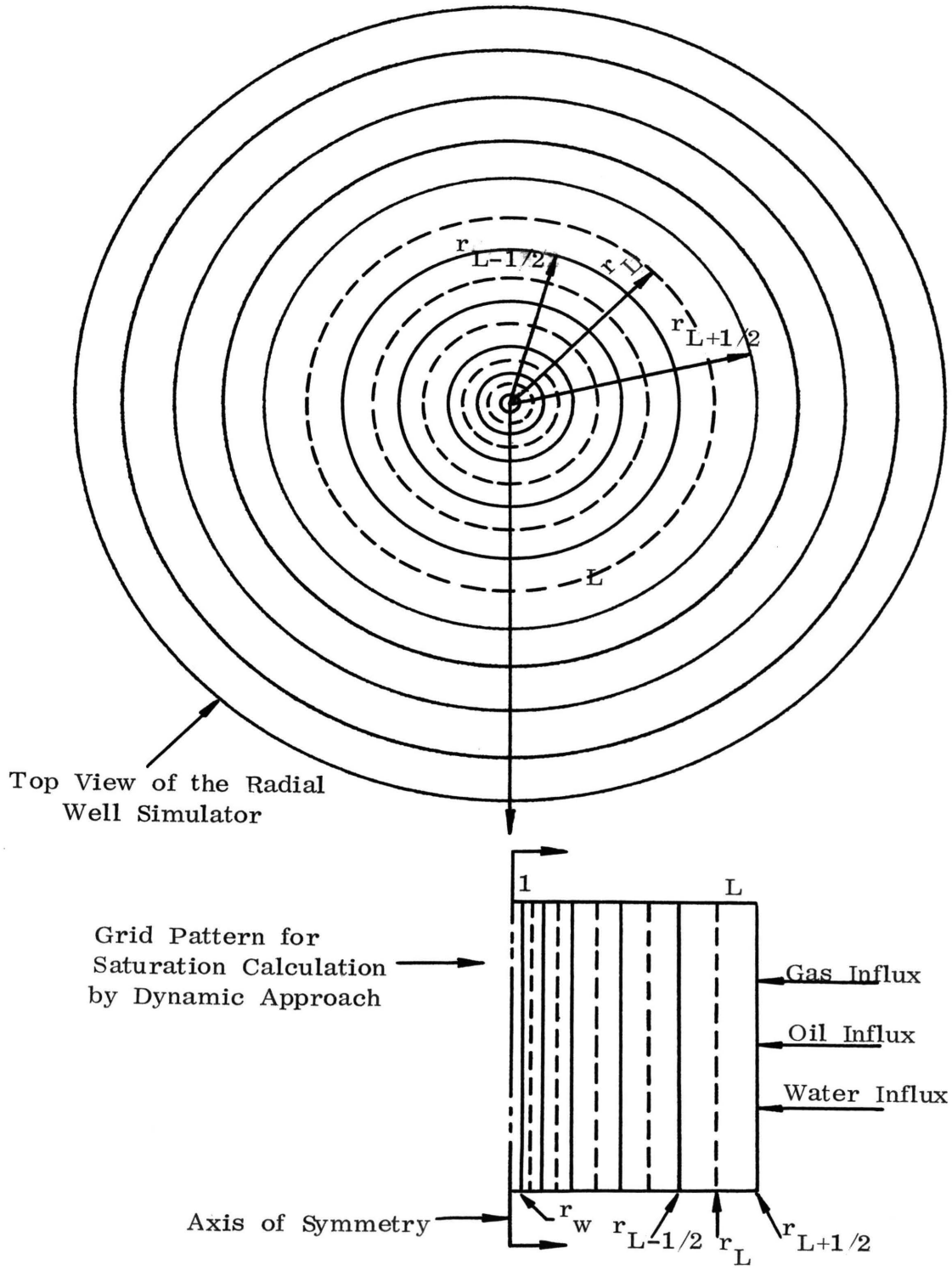

Figure 6. Relation of Grid Pattern for Saturation Calculation by Dynamic Approach to Radial Well Simulator

material balance equations used in this study is presented in Appendix D. Although these equations are somewhat complex, the concept of the material balance can be readily illustrated without use of mathematics. For example, the material balance for total gas must satisfy the following statement of the law of mass conservation:

(gas in) + (gas in place at the old time level) - (gas produced)

= (gas in place at the new time level).....(16)

where total gas is defined as the sum of free gas and solution gas.

Although the relationship expressed by Equation (16) is self-evident, it is not always satisfied by standard computational techniques throughout the simulation model. The source of this problem lies in the vast difference in the sizes of the grid elements within the radial model. For example, the innermost radial element might contain only 0.001 percent of the total pore volume of the radial simulator. The minute sizes of the inner grid elements brings about a situation in which the standard flux balance for these elements is influenced more by machine round-off error than by changes in saturation. Thus, the saturations calculated are entirely meaningless; they are often negative or greater than one hundred percent. These errors lead to unstable pressure calculations in the standard radial model.

The new method utilizes a dynamic concept which calculates first

the gas-oil ratio required to maintain the mass balance for gas in the entire radial model. In terms of Equation (16), the unknown parameter is considered to be gas produced. Accuracy of the first estimate of implicit gas saturations for the innermost grid elements is of little importance, since the pore volume of these radial cells is negligible when compared with the total pore volume of the model. Therefore, the round-off error which causes instability in the standard calculations is not troublesome in the dynamic approach.

After calculating gas-oil ratio, the gas-oil relative permeability may be determined. This ratio is computed by the following equation:

$$\left(\frac{K_g}{K_o}\right)^{n+1}_i = \left\{ G_{in} + \frac{1}{\Delta t} \sum_{k=i}^{L} \left[PV^n \left(\frac{S_g}{\beta_g} + \frac{S_o R_s}{\beta_o}\right)^n \right]_k \right.$$

$$\left. - \frac{1}{\Delta t} \sum_{k=i}^{L} \left[PV^{n+1} \left(\frac{S_g}{\beta_g} + \frac{S_o R_s}{\beta_o}\right)^{n+1} \right]_k - R_{s_i}^{n+1} q_{o_i}^{n+1} \right\}$$

$$\left(\frac{\mu_g \beta_g}{q_o \mu_o \beta_o}\right)^{n+1}_i \qquad \text{.....(17)}$$

$$i = 1, 2, \ldots, L$$

$$q_{o_{i+1}}^{n+1} = q_{o_i}^{n+1} + \frac{\partial}{\partial t} \left[\frac{(PV)S_o}{\beta_o} \right]_i \quad \ldots\ldots\ldots\ldots\ldots\ldots (18)$$

Gas saturation may now be computed, since

$$S_g = f\left(\frac{k_g}{k_o}\right), \qquad S_g > S_{g_c} \quad \ldots\ldots\ldots\ldots\ldots\ldots (19)$$

The relative permeability for each phase was assumed to be a function of the phase saturations. Therefore, the function describing gas saturation in Equation (19) varies with both gas and oil saturations. The complexity of these relationships is such that it was not feasible to obtain a direct solution for S_g. Therefore, an iterative approach was used to obtain gas saturation.

Water influx into the well was not studied, and the complications arising when three phases flow into the radial model were not examined. Therefore, the solution of Equation (19) was sufficient to specify all three saturations for the system which was examined. In this study water saturation remained at its irreducible value, and oil saturation was computed by requiring that the sum of the three saturations be unity:

$$S_{o_i}^{n+1} = 1 - S_{g_i}^{n+1} - S_{w_i}^{n+1} \quad \ldots\ldots\ldots\ldots\ldots\ldots\ldots\ldots (20)$$

The solution scheme required that the saturation in the first block be calculated initially by Equations (17) and (19), on the basis of the oil production rate into the well bore. The gas flux in, G_{in}, was computed from the standard radial model and was the total gas entering its inner block from the adjacent block. This gas flux was calculated from upstream relative permeabilities. The inner grid element was relatively large in the standard radial model, and it was subdivided logarithmically to form the grid system for the dynamic model. This scheme is illustrated in Figure 6.

After the saturations were calculated in block 1 of the dynamic model, the oil production rate was adjusted for accumulation using Equation (18), and transferred to block 2. Oil and gas saturations were then calculated for block 2.

This procedure was repeated sequentially through block L. The technique has been shown by tests described in this study to be a stable method for computing saturations in the small inner elements of the radial grid. Stability was maintained even for the simulation of reservoir behavior within a few inches from the producing sand face. Pressure at the sand face was calculated by extrapolation using Equation (12).

V. VALIDATION CRITERIA

Since the radial model represents a rectangular grid block in the areal model, it was necessary to establish criteria for equivalence of the two systems. One criterion which was selected is that the pore volume of the radial model must equal the pore volume of the rectangular block. Since the porosity and bed thickness in the radial model equal the corresponding terms in the areal model, the external radius of the well simulator was calculated by

$$r_e = \sqrt{\Delta x_i \Delta y_j / \pi} \quad \ldots\ldots\ldots\ldots\ldots\ldots\ldots\ldots\ldots\ldots\ldots\ldots\ldots\ldots\ldots\ldots (21)$$

The effect of relative sizes of Δx_i and Δy_j on accuracy of the simulation has not been investigated. However, since the circular shape of the radial model corresponds more closely to a square than to a rectangle, this study was made with $\Delta x_i = \Delta y_j$ for grid blocks which contain wells in the areal reservoir model. The use of square grid blocks near producing wells is consistent with conventional modeling techniques. It is customary to utilize rectangular grid spacing only for representation of the reservoir system at points remote

from the area of primary interest.

Another criterion which was selected to assure correspondence of the two models is that the volumetrically weighted average pressure within the radial model must equal the corresponding block pressure in the areal model. Since accumulated round-off error could eventually cause a discrepancy in pressures calculated by the two models, pressures in the radial model were automatically adjusted to maintain the desired equivalency with areal model pressure. These small adjustments were made without altering the pressure gradients calculated by the radial model. These adjustments were based on the following equations:

The volumetrically weighted average pressure ($\overline{P}_R$) for the radial model was calculated by

$$\overline{P}_R = \frac{\sum_{i=1}^{I} \frac{PV_i S_{o_i} P_i}{\beta_{o_i}}}{\sum_{i=1}^{I} \frac{PV_i S_{o_i}}{\beta_{o_i}}} \quad \ldots\ldots\ldots\ldots\ldots\ldots\ldots\ldots (22)$$

The term PMP is the difference between $\overline{P}_R$ and the block pressure of the grid that contains the well in the areal model. This difference was substracted from each pressure in the radial model. This procedure is shown by the following two equations:

$$PMP = \bar{P}_R - (P_{i,j})_A \quad \ldots\ldots\ldots\ldots\ldots\ldots\ldots\ldots\ldots\ldots\ldots\ldots (23)$$

and

$$(P_i)_R^{k+1} = (P_i)_R^k - PMP \quad \ldots\ldots\ldots\ldots\ldots\ldots\ldots\ldots\ldots\ldots\ldots\ldots (24)$$

where the subscripts A and R denote areal and radial models, respectively. Following this adjustment in the radial model, it was essential to reduce pressure residuals in Equation (10) by the residual relaxation method discussed previously. The saturation computations were begun after the radial model pressure residuals were reduced to an appropriate level.

If the radial model is to represent the system predicted by the areal simulator, then the fluid fluxes must be the same for both models. This condition was achieved by summing the fluxes into the four vertical faces of the grid block in the areal model, and considering the total flux for each phase as influx into the closed outer boundary of the radial model, as was discussed in Chapter III. It should be noted that small errors in calculating pressures in the areal model may invalidate the flux calculation. Therefore, the pressure residuals in the areal model were reduced to a low level.

Gas production rates from the radial model were then determined by gas-oil mobility ratio relationship, and production rates for this model were compared with corresponding production rates predicted by

the areal model. If these rates were found to differ significantly between the two models, areal model pressure calculations were repeated using production rates calculated by the radial model. This iterative process was repeated until the two models predicted the same fluid production rates. Convergence was usually obtained with one iteration. It should be noted that instability occurs only when the radial model calculation becomes somewhat unstable and predicts high gas saturation. It has been found that the dynamic saturation calculation method corrects this situation.

It should be noted that the method of computation can lead to an ambiguous situation. The radial model may predict production of free gas while the areal model indicates that the block pressure is greater than bubble-point pressure. This situation arises because the areal model fails to provide an adequate simulation of reservoir conditions near the well bore. The problem was handled by two different methods, and both methods gave good results. The first method handled the problem by comparing free gas production predicted by the two models. Any excess gas predicted by the radial model was considered as additional solution gas production in the areal model. Since the material balance must be maintained in each model, R_s in the areal model was reduced to account for this excess gas production.

The second method handled the problem by comparing the total gas in the grid block of the areal model with the total gas

of all the cells of the radial model. Since accumulated round-off error could eventually cause a discrepancy in pressures calculated by the two models, gas saturations in the radial model were automatically adjusted to maintain equivalency of total gas in the two models. Total gas volume error between the two models was also calculated, and it was found to reduce with gas saturation adjustments.

The total gas volume for the areal block (GVA) was calculated by

$$GVA = \left[\frac{PV_{i,j} S_{g_{i,j}}}{\beta_{g_{i,j}}} + \frac{PV_{i,j} S_{o_{i,j}} R_{s_{i,j}}}{\beta_{o_{i,j}}} \right]_A \quad \ldots\ldots\ldots\ldots (25)$$

Total gas volume for the radial model (GVR) was calculated by

$$GVR = \sum_{i=1}^{I} \left[\frac{PV_i S_{g_i}}{\beta_{g_i}} + \frac{PV_i S_{o_i} R_{s_i}}{\beta_{o_i}} \right]_R \quad \ldots\ldots\ldots\ldots\ldots (26)$$

The gas volume error (GVE) between the two models was defined as

$$GVE = \left(1 - \frac{GVR}{GVA}\right) \times 100 \quad \ldots\ldots\ldots\ldots\ldots\ldots\ldots\ldots\ldots (27)$$

The gas saturations in the radial model were adjusted according to the equation

$$(S_{g_i})^{k+1}_R = (S_{g_i})^{k}_R - GMG \quad \ldots\ldots(28)$$

where $$GMG = SR - (S_{g_{i,j}})_A \quad \ldots\ldots(29)$$

and

$$SR = \frac{\sum_{i=1}^{I} \left[\frac{PV_i S_{g_i}}{\beta_{g_i}} + \frac{PV_i S_{o_i} R_{s_i}}{\beta_{o_i}}\right]_R - \left[\frac{PV_{i,j} S_{o_{i,j}} R_{s_{i,j}}}{\beta_{o_{i,j}}}\right]_A}{\left[\frac{PV_{i,j}}{\beta_{g_{i,j}}}\right]_A} \quad \ldots\ldots(30)$$

The term SR is a pseudo-average gas saturation for the radial model which caused the iterative adjustment shown by Equation (28) to converge to the correct value. As pointed out earlier, the convergence criterion is that both models contain the same total gas mass.

After each gas saturation adjustment, oil saturation was also adjusted, and pressure adjustment calculations discussed previously were also repeated. This iterative process was repeated until the gas volume error (GVE) was reduced to a very low level. It was found that convergence was rapid, and the maximum number of iterations was approximately five.

A flow chart describing the sequence of calculations is presented in Appendix F.

VI. APPLICATION OF THE MODEL

This chapter describes in the first section the types of models used in the study. This is followed by a presentation and discussion of the results obtained by the test models.

A. Description of Test Systems

The model was applied to a small hypothetical oil field as shown in Figure 7. Rock and fluid properties and well data are described in Appendix E. The reservoir is homogeneous, isotropic, and uniform in thickness. As illustrated in Figure 7, development consists of two producing wells and sufficient dry holes to define the limits of the oil field. The field is divided into one hundred grid elements (10 x 10). Each element is square with $\Delta x = \Delta y = 528$ feet.

Water and oil saturations were initially distributed according to the capillary pressure curve, shown by Figure 4A in Appendix E. The reservoir was initially above bubble-point pressure. Both grid sections containing producing wells were taken for a detailed well analysis. Each well was assumed to be in the center of the areal block, and was represented by a radial model which was divided into fourteen radial cells.

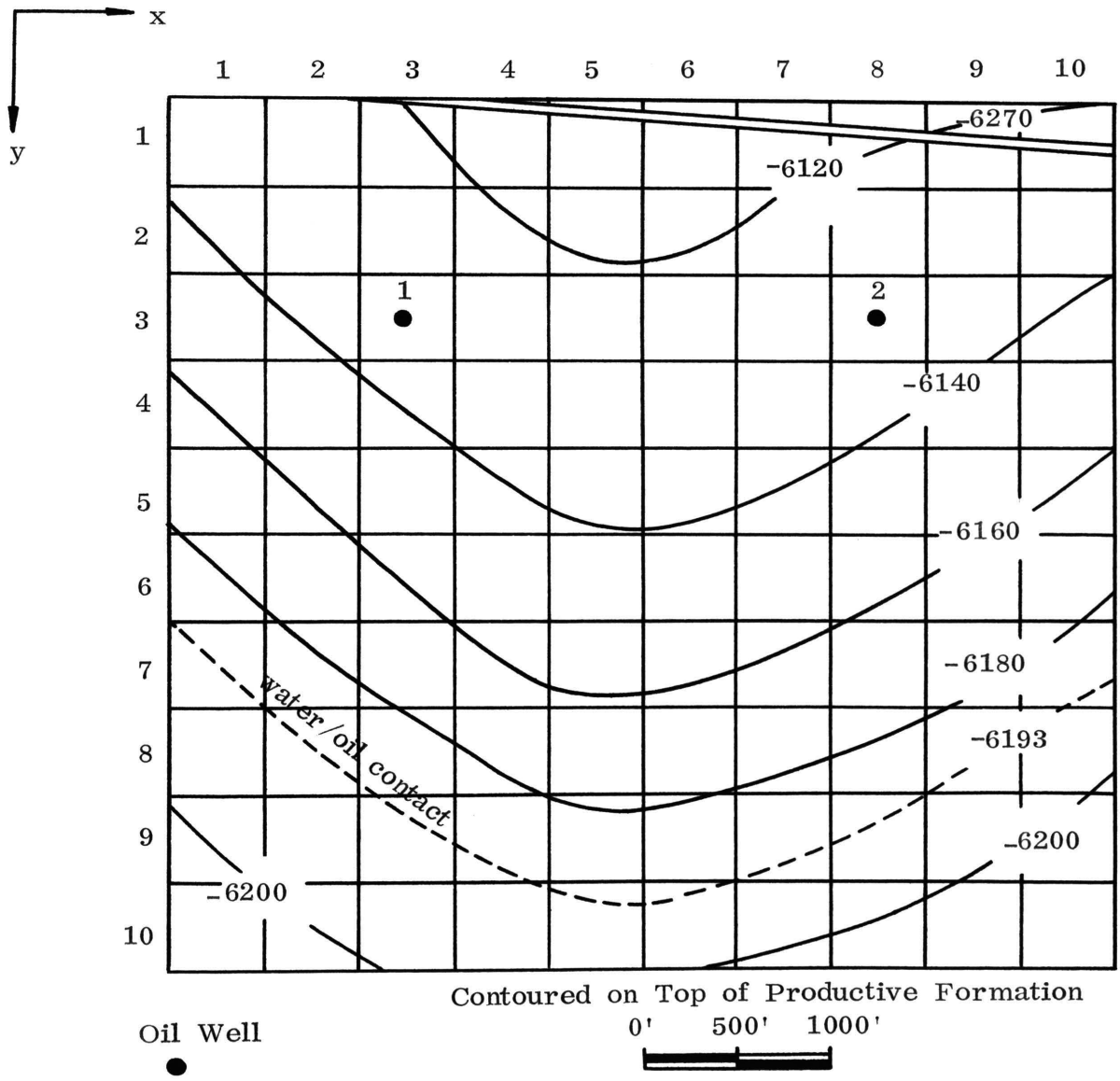

Figure 7. Structural Map of Hypothetical Oil Field

Fine grid spacing was used near the well bore to obtain better definition of pressure and saturation profiles in this critical region. This was done by dividing the first five cells into logarithmic increments, increasing in size away from the well bore. The outer nine grid elements were divided into equal increments of Δr. The dimensions of these increments are listed in Appendix E.

It was assumed that each well would produce at an allowable rate of 197 barrels per day until bottom-hole pressure was reduced to 200 psia. Thereafter, bottom-hole pressure was held constant at 200 psia, and the wells produced at maximum capacity, which was calculated by the standard approach discussed in Chapter III.

In order to compare results obtained by the dynamic material balance technique with those obtained by standard approaches, three test models were used for the same field. The first test was made with a standard radial model simulating well performance in the areal model. The second was made by including the dynamic technique in the radial model near the well bore. A third test was made using only an areal model with bottom-hole pressure calculated from Darcy's law in radial coordinates.

In addition to the three tests described above, another test was conducted to study the capability of the well simulator to obtain pressure build-up data. This procedure tests the validity of the unsteady-state model

and yields a basis for matching field results. This test was conducted by closing well No. 1 at the sand face and allowing the fluxes at the outer faces of the areal model to continue to flow into the well simulator for a short period of time (0.001 day).

The comparison tests for the three models indicated that results were different for each model. The combined areal and standard radial model was not sufficiently stable to produce conclusive results. The simulation of well bore effects using the combined areal and radial models with the dynamic material balance technique yielded results which differed from those obtained with the standard areal model, which has no capability of accounting for the reduction of oil permeability near the well bore. The simulated pressure build-up test was also successful. These results are described in the following section.

B. Results

The three tests referred to in the previous section each consisted of several computer runs made with the corresponding simulation systems. Test No. 1 refers to those results obtained using the combined areal-standard radial model system. Test No. 2 consists of results obtained from combined areal-radial-dynamic material balance model system; this system is referred to hereafter as the dynamic model. Test No. 3 was made with the areal model only, using Darcy's law to calculate bottom-hole pressures in the well. The other test on pressure build-up

referred to in the previous section was actually a part of Test No. 2; it is discussed separately as the pressure build-up test.

Results for Test No. 1 are presented in Tables I through III for three different runs made with this model. The results of this test consist only of values of stability criteria used in the study. These are presented to show how a standard approach failed to simulate bottom-hole pressure. These runs were conducted with various inner block sizes and various time steps. The results of run No. 1 are presented in Table I. These results were obtained with an inner block radius (r_1) of 1.7 feet and a time step size of 0.01 day. Instability of gas saturation appeared at 0.34121 year, and the material balance became unstable thereafter. The time step size was reduced in order to improve stability, and a stable solution was found with $\Delta t = 0.0001$ day. Table II shows the results of the second run which was made with a larger inner block radius of 14.7 feet and with a time step of 2 days. Instability in gas saturation was apparent at 0.5593 year, and the sum of saturations in the inner blocks became approximately 95.5% and fluctuated thereafter. The time step size was decreased and a stable solution was obtained for a time step of 0.01 day. Table III presents the results of the third run with an inner block radius of 45 feet and a time step of 6 days. Signs of instability appeared at 0.9781 year. A stable solution was found with a time step of 4 days. Other parameters shown in the tables are defined immediately after Table I. These parameters are validity criteria

TABLE I

Results of Combined Areal and Conventional Radial Models for r_1 = 1.7 feet and Δt = 0.01 day

Time, Years	Gas Saturation in Producing Block, %	GVE* %	GMG* %	PMP* Psia	Sum of Saturations
0.1091	0.0	0.0000189	-0.0000754	- 15.0	0.9975
0.3411	5.71	-2.226	0.00853	- 34.0	1.0293
0.34112	6.53	-1.074	0.0041211	25.5	0.9766
0.34115	11.19	0.6819	-0.002397	15.0	1.0294
0.34118	14.48	-1.4360	0.005488	- 32.0	0.9904
0.34121	21.41	1.362	-0.005224	-184.0	1.0373
0.34123	-11.2429	-9.290	0.035625	328.0	0.0162
0.34126	-39.69	3.476	-0.013310	165.0	-3.6135

* The following equations describe the parameters GVE, GMG, and PMP that are listed in the Table.

$$GVA = PV_{i,j}\left[S_{g_{i,j}}/\beta_{g_{i,j}} + S_{o_{i,j}} R_{s_{i,j}}/\beta_{o_{i,j}}\right] \quad \text{Areal}$$

$$GVR = \sum_{i=1}^{I}\left[PV_i S_{g_i}/\beta_{g_i} + PV_i S_{o_i} R_{s_i}/\beta_{o_i}\right] \quad \text{Radial}$$

$$GVE = (1. - GVR/GVA) \times 100$$

where, GVA = total gas volume in the areal block

GVR = total gas volume in the radial model

$$GMG = \left\{\left[GVR - (PV_{i,j} S_{o_{i,j}} R_{s_{i,j}}/\beta_{o_{i,j}})_{Areal}\right]/(PV_{i,j}/\beta_{g_{i,j}})_{Areal}\right\} - (S_{g_{i,j}})_A$$

$$PMP = \sum_{i=1}^{I}\left[(PV_i S_{o_i} P_i/\beta_{o_i})/\sum_{i=1}^{I}(PV_i S_{o_i}/\beta_{o_i})\right]_R - (P_{i,j})_A$$

TABLE II

Results of Combined Areal and Conventional Radial Models for r_1 = 14.7 feet and Δt = 2 days

Time, Years	Gas Saturation in Producing Block, %	GVE %	GMG %	PMP Psia	Sum of Saturations
0.3251	0.0	-0.0000186	0.00000112	- 0.06732	1.0000
0.4132	5.3	0.00972	-0.000763	0.5321	1.0024
0.5593	28.43	6.86	-0.002397	18.4828	0.9941
0.5647	76.15	-6.338	0.002238	16.344	0.9951

TABLE III

Results of Combined Areal and Conventional Radial Models for r_1 = 45 feet and Δ t = 6 days

Time, Years	Gas Saturation in Producing Block, %	GVE %	GMG %	PMP Psia	Sum of Saturations
0.4011	0.0	-0.0001907	0.00001151	-1.32079	1.00000
0.4285	0.7	-0.08401	0.00001261	-0.004083	1.0000
0.4421	1.0	-0.10938	0.00003981	-0.00535	1.0000
0.4832	1.7	-0.16345	0.0000673	-0.0081526	1.0000
0.7019	5.3	0.009924	-0.000561	5.8757	1.0003
0.896	7.8	2.5884	-0.009723	38.22	1.0059
0.9616	10.2	1.47948	-0.00574	26.46	1.0019
0.9781	30.16	6.85573	-0.02674	99.9	0.9979
0.9945	54.65	-0.74377	0.002905	-19.8	1.0001
1.010	31.17	6.515	-0.02548	92.6	0.9977
1.027	42.45	2.4201	-0.009477	13.4	1.0017
1.043	60.54	0.8116	-0.003182	17.5	0.9996
1.0598	56.62	0.2607	-0.001023	6.2	0.9997
1.0762	62.73	0.9236	-0.003632	18.3	1.0000
1.0926	-206.9	239.8	-0.9482	-3405.	-1.4323

that indicate accuracy of the linkage of the well simulator with the corresponding areal block; they are also indicators for material balance stability in the radial model. These criteria were poor for Test No. 1, and this approach was abandoned because of the lack of resolution of the method, which results from the large block sizes. Furthermore, the method is computationally inefficient because of the small time steps which must be used. The technique is presented here for the purpose of comparing a combination of standard models with the model built from the new concepts in material balance calculations.

Results for Test No. 2 and Test No. 3 are presented in Table IV, and Figures 8 through 16. Table IV shows the results of the dynamic material balance approach with an inner radius (r_1) of 0.81 feet and a time step of 10 days. As indicated in Table IV, a stable solution was obtained for gas saturation, and the deviation of the sum of saturations from unity never exceeded 0.01%. Increasing the time step size to 30 days did not cause the solution to become unstable. This technique was found to be successful in achieving stable material balance calculations. These results also indicate that the linkage of the radial and the areal models is valid. The greatest deviation between the average pressure of the radial model and the corresponding areal block is 1.115 psi. The value occurred only once during the simulation. These deviation values can be reduced to any desirable tolerance by the iterative scheme discussed in the previous chapter.

TABLE IV

Results of Combined Areal and Radial Models using Dynamic Approach for $r_1 = 0.81$ feet and $\Delta t = 10$ days

Time, Years	PMP, Psia	GMG, %
0.130	0.0	0.01197
0.213	0.0	0.01236
0.308	0.1526×10^{-4}	0.0177
0.404	-0.1526×10^{-4}	0.0224
0.500	-0.1526×10^{-4}	0.00925
0.609	0.30517×10^{-4}	-0.00826
0.7185	0.30517×10^{-4}	-0.00434
0.8005	-0.1525×10^{-4}	-0.00512
0.9099	0.61035×10^{-4}	0.00576
1.0466	0.3051×10^{-4}	-0.0067
1.2517	0.3051×10^{-4}	-0.008612
1.4565	0.12207×10^{-3}	-0.0065709
1.5522	0.28541	-0.004696
1.6890	0.36280	-0.00905
1.7847	0.41480	-0.00799
1.9077	0.47204	-0.006745
2.0034	0.51693	-0.005698
2.2495	0.6323	-0.005842
2.454	0.84854	0.0087457
2.8098	0.952179	0.006159
3.2063	1.115	0.006227

Figure 8 shows the percentage gas volume error (GVE) between the linked models as a function of time. It indicates success in linking the two models, and it shows indirectly the stability in the saturation computation technique used for the radial model. Table IV and Figure 8 indicate the validity and applicability of such a simulation model to the study of individual well performance in a field simulation model. These two combined models were used to study well performance for the reservoir example described in the previous section.

Although the same criteria were used to determine reservoir behavior for the two methods of simulation (described as Tests No. 2 and No. 3), significant differences in predicted reservoir performance were observed. As illustrated by Figure 9, the dynamic model (Test No. 2) predicts an early build-up in gas saturation near the production wells, whereas the areal model (Test No. 3) without the radial simulator does not anticipate this effect. Figures 10 and 11 depict the producing bottom-hole pressure and productivity index, respectively, as calculated by the two types of simulation models. Figure 12 indicates the calculated pressure distribution in the vicinity of well No. 1. Oil production rates and calculated gas/oil ratio are illustrated by Figure 13 and 14 respectively. As illustrated by Figure 15, the dynamic model predicts a lower oil recovery per well than the areal model.

The result of the simulated pressure build-up test is shown in

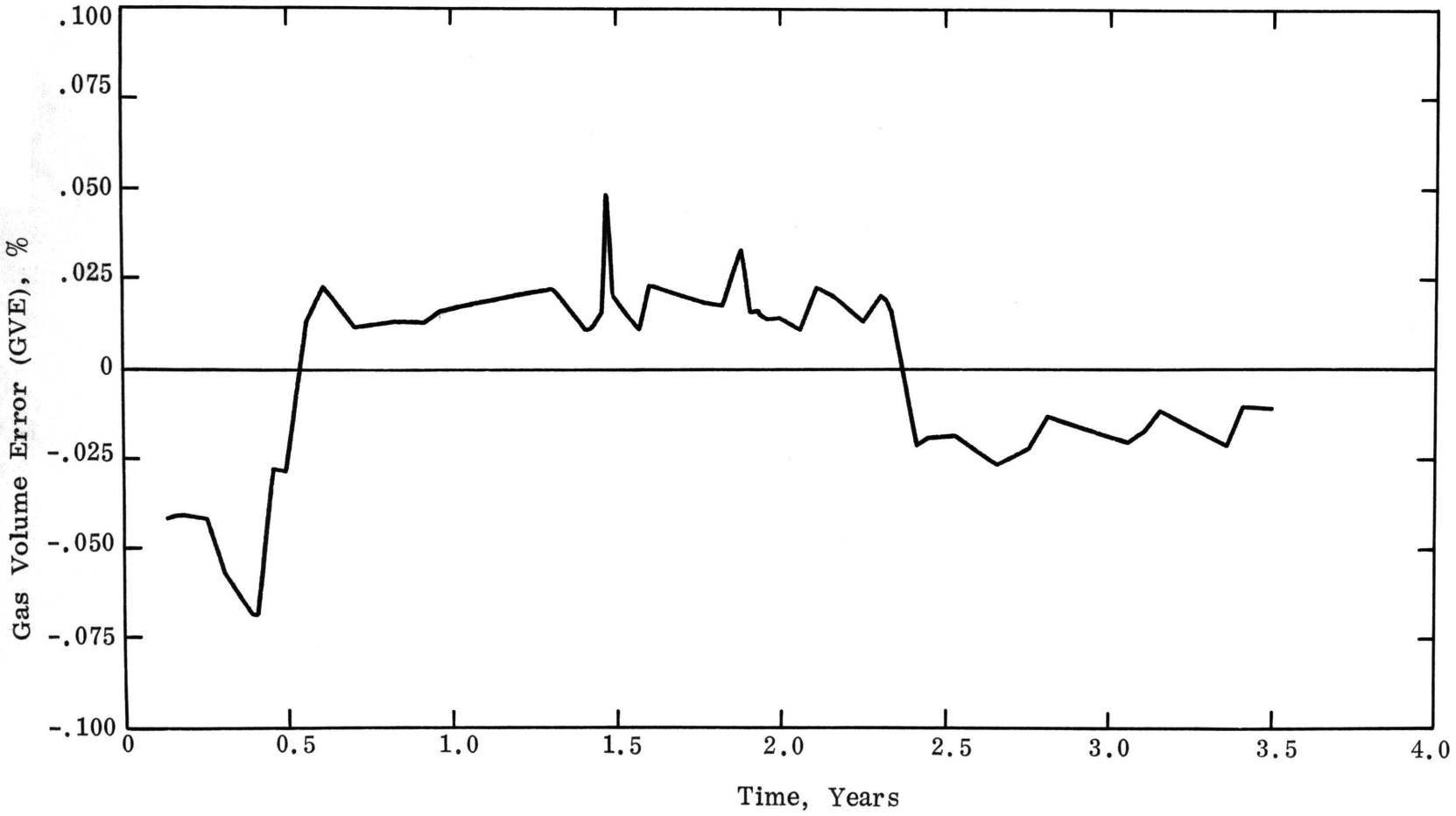

Figure 8. Calculated Gas Volume Error for Dynamic Model, Well No. 1

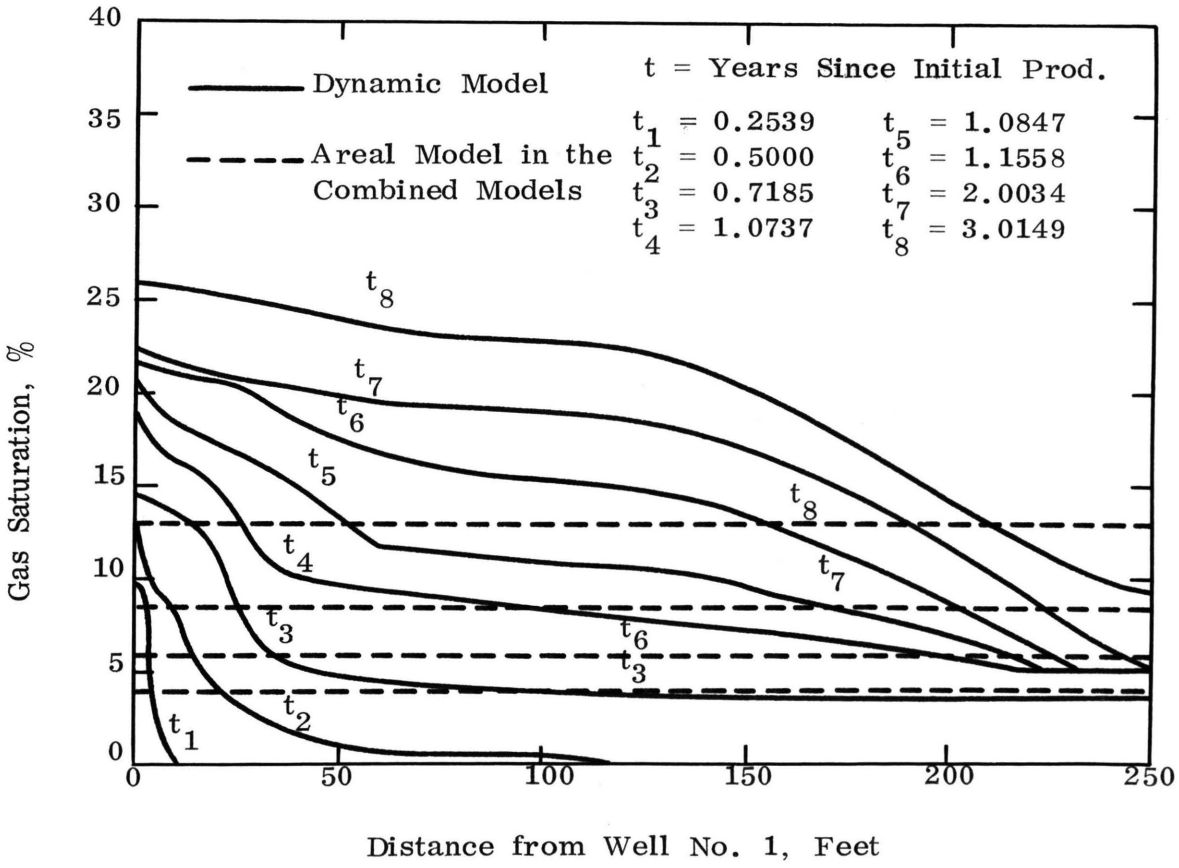

Figure 9. Calculated Gas Saturation Distribution, Well No. 1

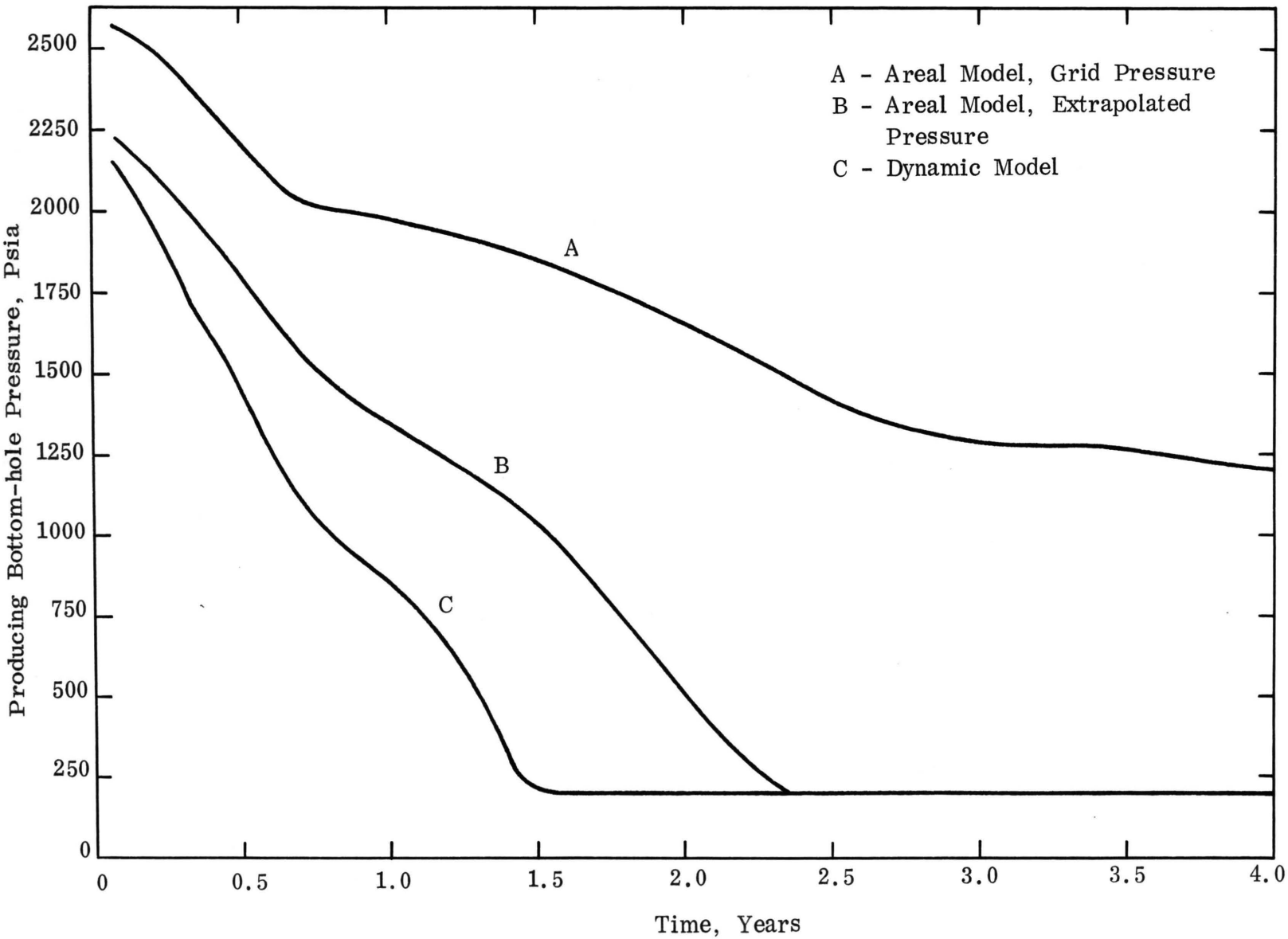

Figure 10. Calculated Producing Bottom-hole Pressure, Well No. 1

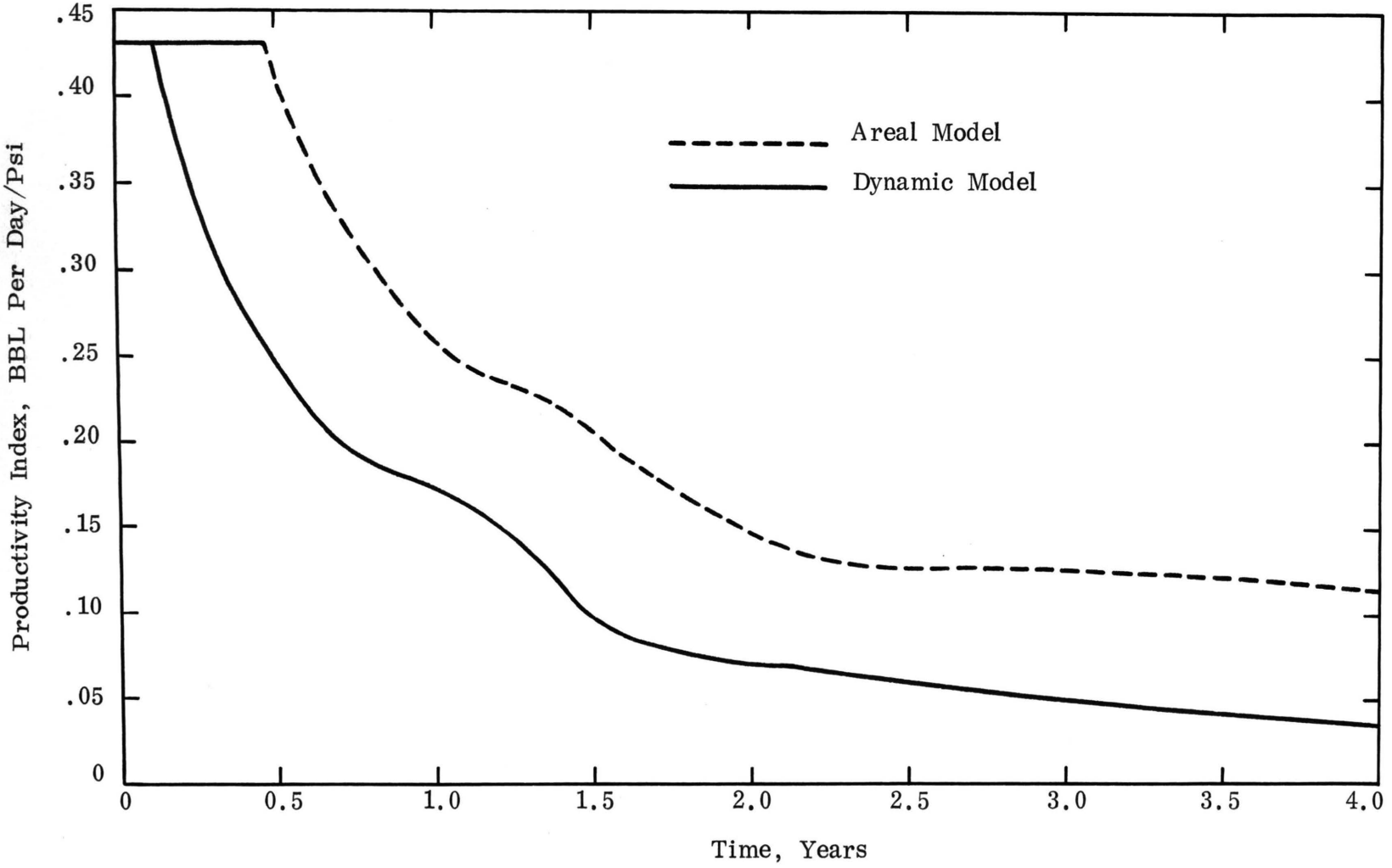

Figure 11. Calculated Productivity Index, Well No. 1

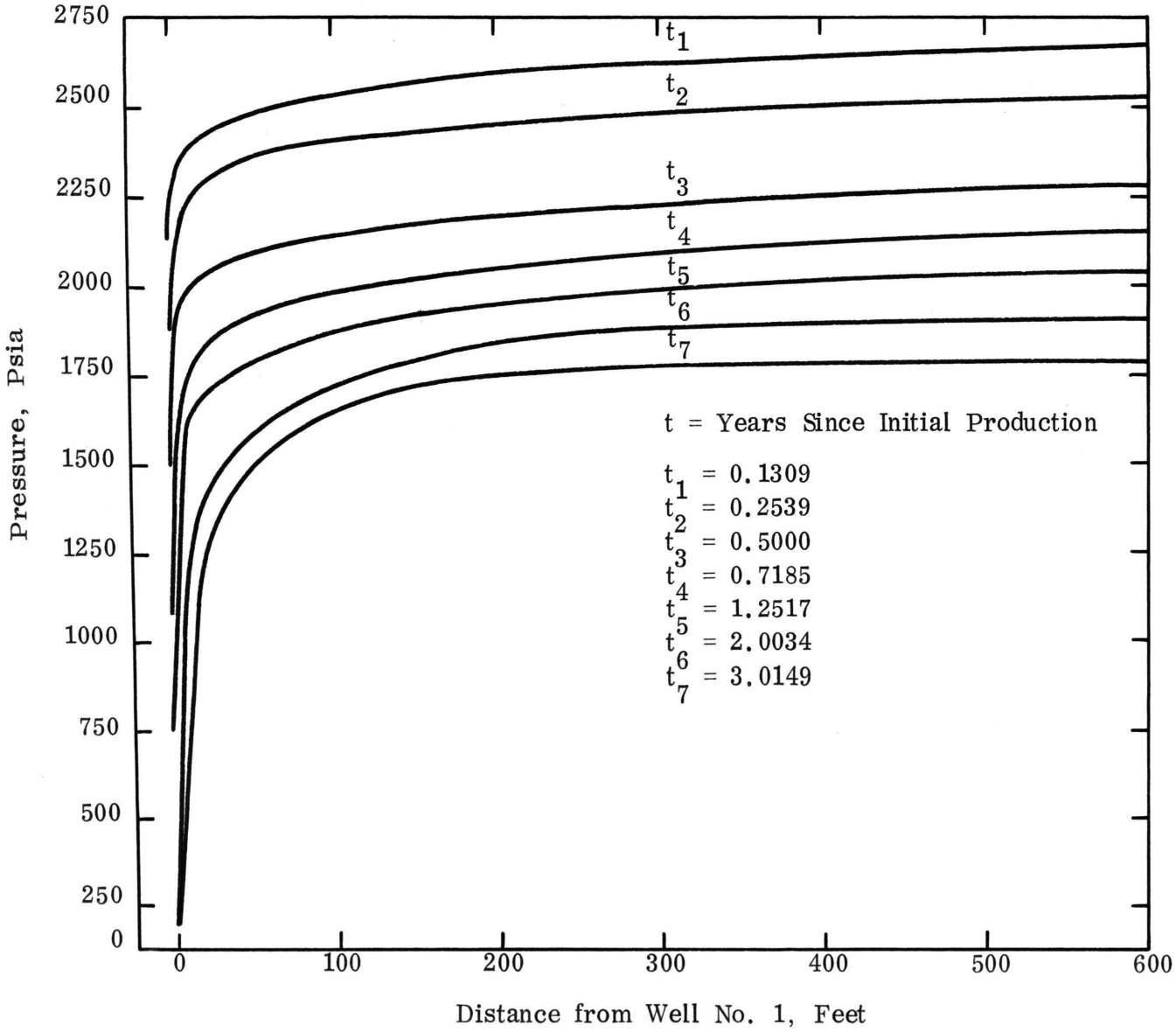

Figure 12. Calculated Pressure Distribution, Well No. 1

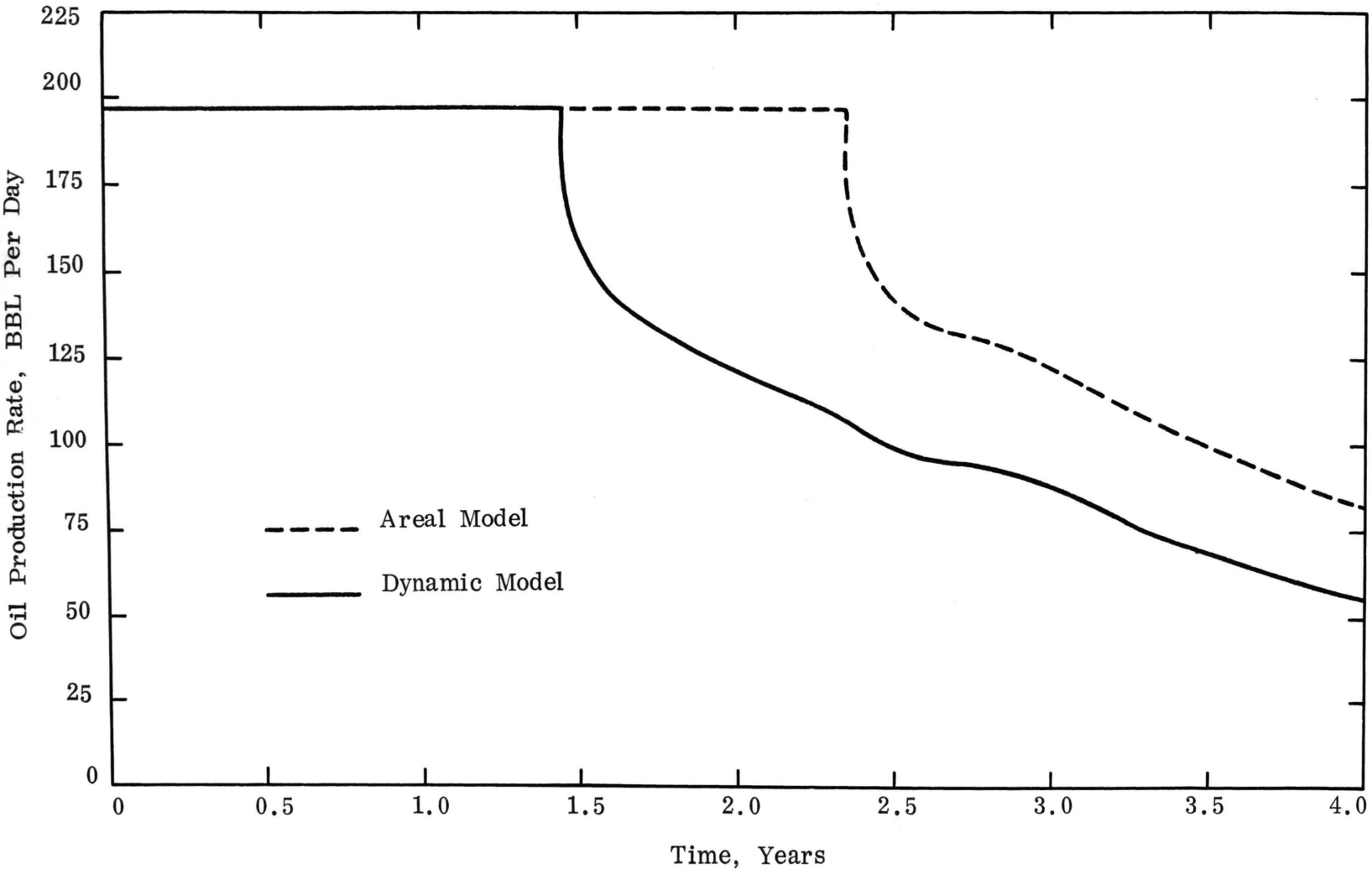

Figure 13. Calculated Oil Production Rate, Well No. 1

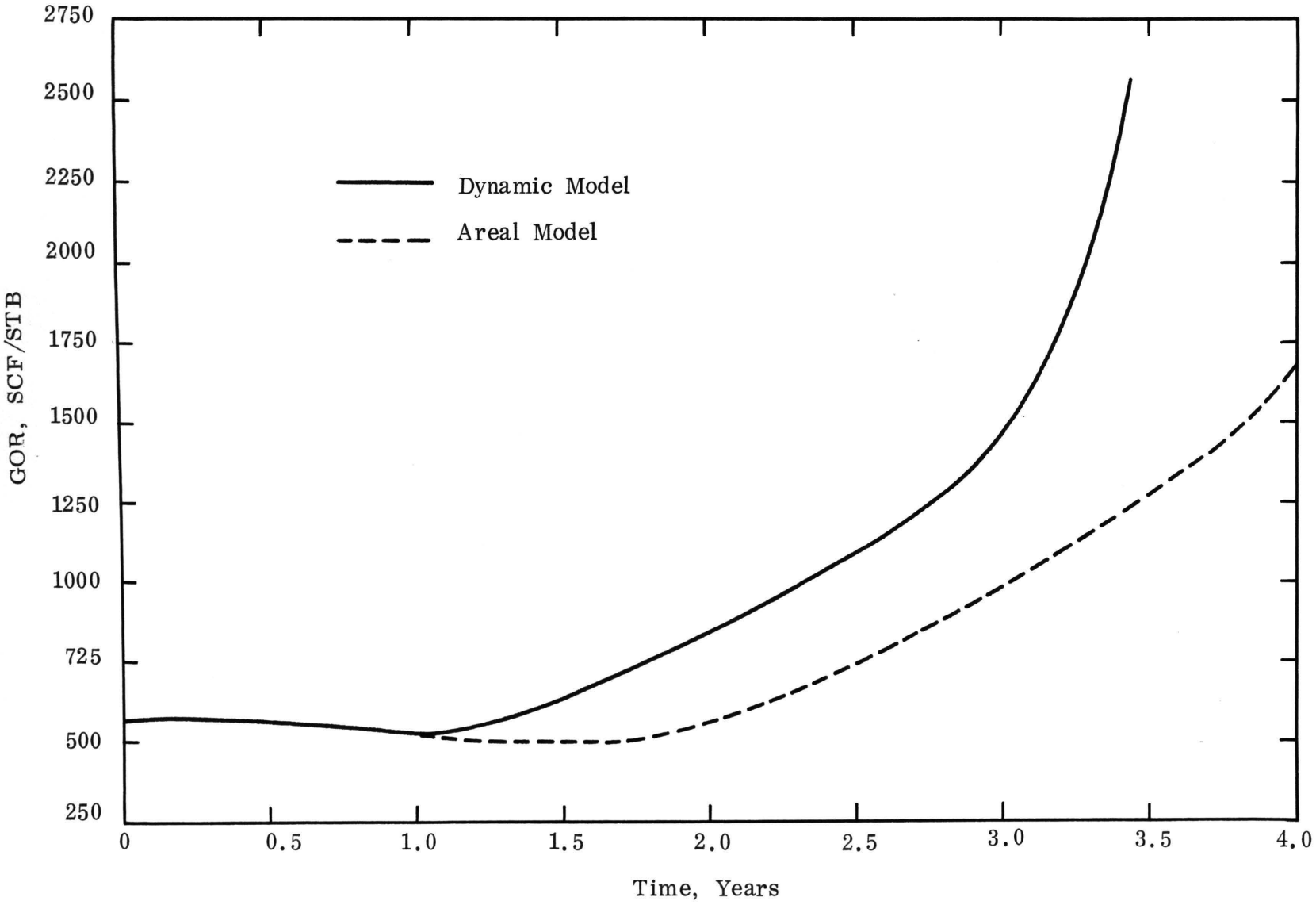

Figure 14. Calculated Gas/Oil Ratio, Well No. 1

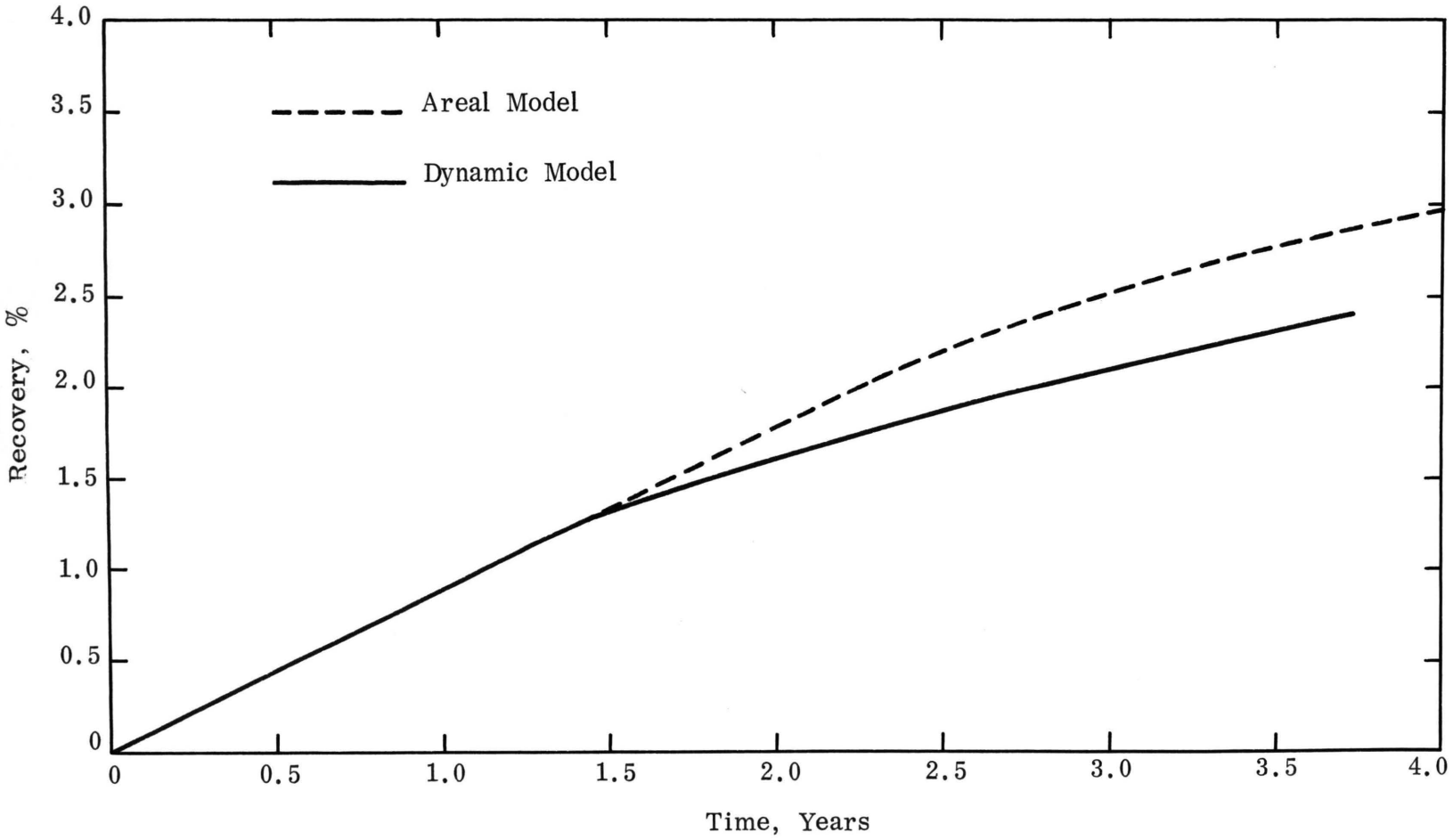

Figure 15. Percent Recovery of Original Oil in Place, Well No. 1

Table V. Figure 16 is the pressure build-up curve for well No. 1, after a production period of 0.5547 year (4860 hours).

These models were run on the IBM 360/50 digital computer. Use of the dynamic model increased computation time by approximately 27% as compared with the standard areal model. The example used required 10.5 seconds of computer time per time step for the areal model, and 13.35 seconds of computer time per time step for the dynamic model.

TABLE V

Simulation Data for Pressure Build-up Analysis

Hours	$\frac{t_s^* + \Delta t}{\Delta t}$	P Psia
.05	97201	1575
.50	9721	2154
1.00	4861	2172
2.00	2431	2190
4.00	1216	2221
8.00	608	2232
12.00	406	2238
16.00	304	2242
20.00	244	2245
24.00	203	2248
28.00	175	2250
32.00	153	2251
36.00	136	2253
40.00	122	2254
44.00	111	2256
48.00	102	2257

* Flowing time before shut in t_s = 4860 hours.

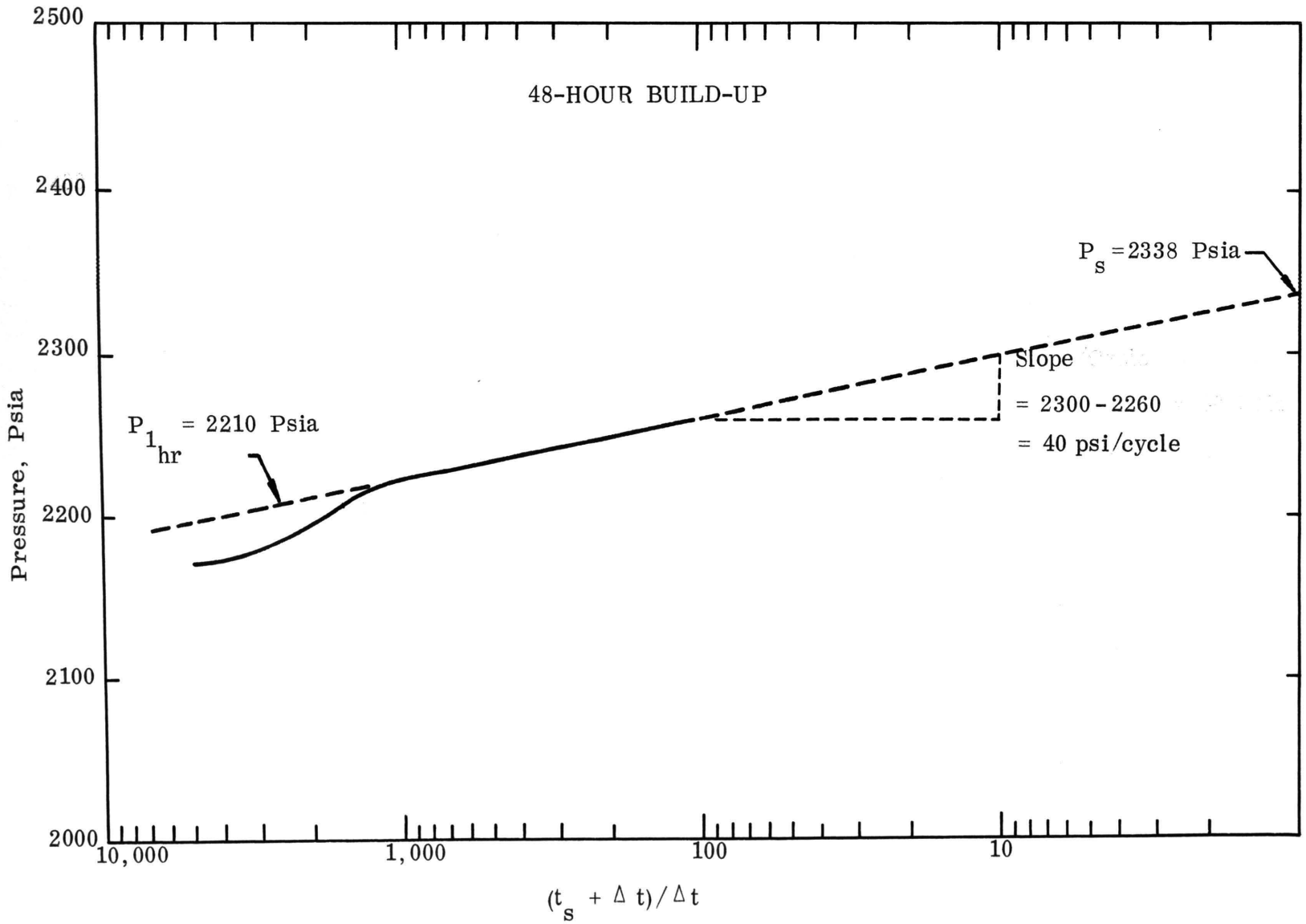

Figure 16. Simulated Pressure Build-up Curve, Well No. 1

VII. CONCLUSIONS

The following conclusions were reached on the basis of this investigation:

1. The validity criteria which were studied showed that it is feasible to link a radial model to an areal model for the purpose of simulating well performance.

2. Stability tests for a radial model using the dynamic material balance approach developed in this work show that this new method is stable and accurate for reasonably large time steps and for fine grid spacing near the well.

3. This technique is suitable for commercial use. In this study the new model increased computing time by only 27% for two wells in a (10 x 10) grid system, and it gave well performance information which cannot be obtained by conventional simulation methods.

4. It is suggested that this type of model be employed to study reservoirs where pressure drawdown at producing wells is

large, and bottom-hole pressures are less than bubble-point pressure.

REFERENCES

1. Douglas, J., Jr., Peaceman, D. W., and Rachford, H. H., Jr.: "A Method for Calculating Multidimensional Immiscible Displacement", Trans. AIME, (1959), vol. 216, p. 297.

2. West, W. J., Garvin, W. W. and Sheldon: "Solution of the Equations of Unsteady-State Two-Phase Flow in Oil Reservoirs", Trans. AIME, (1954), vol. 201, p.217.

3. Coats, K. H., Neilson, R. L., Terhune, M. H. and Weber, A. G.: "Simulation of Three-Dimensional, Two-Phase Flow in Oil and Gas Reservoirs", Soc. Pet. Eng. J., (December, 1967), p. 377.

4. Fagin, R. G. and Stewart, C. H., Jr.: "A New Approach to the Two-Dimensional, Multi-phase Reservoir Simulator", Soc. Pet. Eng. J., (June, 1966), p. 175.

5. Cavendish, J. C., Price, H. S. and Varga, R. S.: "Galerkin Methods for the Numerical Solution of Boundary Value Problems", Soc. Pet. Eng. J., (June, 1969), p. 204.

6. vanPoollen, H. K., Breitenbach, E. A. and Thurnau, D. H.: "Treatment of Individual Wells and Grids in Reservoir Modeling", Soc. Pet. Eng. J., (December, 1968), p. 341.

7. Welge, H. Y. and Weber, A. G.: "Use of Two-Dimensional Methods for Calculating Well Coning Behavior", Soc. Pet. Eng. J., (December, 1964), p. 345.

8. Blair, P. M. and Weinaug, C. F.: "Solution of Two-Phase Flow Problems using Implicit Difference Equations", Soc. Pet. Eng. J., (December, 1969), p. 417.

9. MacDonald, R. C. and Coats, K. H.: "Methods for Numerical Simulation of Water and Gas Coning", Trans. AIME, (1970), vol. 249, p. 425-436.

10. Letkman, J. P. and Ridings, R. L.: "A Numerical Coning Model", Soc. Pet. Eng. J., (December, 1970), p. 418.

11. Mrosovsky, I. and Ridings, R. L.: "Two-Dimensional Radial Treatment of Wells within a Three-Dimensional Reservoir Model", SPE Paper #4286 Presented at the Third Numerical Simulation of Reservoir Performance Symposium, Houston, Texas, January 10-12, 1973.

12. Akbar, Ali M., Arnold, M. D. and Harvey, A. H.: "Numerical Simulation of Individual Wells in a Field Simulation Model", SPE Paper #4073 Presented at 47th Annual SPE Fall Meeting, San Antonio, Texas, October 8-11, 1972.

13. Peaceman, D. W. and Rachford, H. H., Jr.: "The Numerical Solution of Parabolic and Elliptic Differential Equations", J. Soc. Indus. Appl. Math., (1955), vol. 3, p. 28.

14. Arnold, M. D. and Achmad, G.: "Pressure Residual Relaxation Method", Personal Communications.

15. Akbar, Ali M.: "Numerical Simulation of One-Dimensional Three-Phase Fluid Flow in a Stratified Petroleum Reservoir with no Cross-Flow", M. S. Thesis, University of Missouri - Rolla, Rolla, Missouri, (December, 1969).

VITA

The author, Ali Mohammed Akbar, was born on April 22, 1941 in Kuwait City, Kuwait. He received his primary education at Al-Ahmadia and Al-Sabah Elementary Schools and his secondary education at Shawaikh Secondary School in Kuwait. He received his Bachelor of Science Degree in Petroleum Engineering in January, 1966 from the University of Tulsa, Tulsa, Oklahoma. He enrolled at the University of Missouri - Rolla as graduate student in September, 1968. He received his Master of Science in Petroleum Engineering in December, 1969, and his Master of Science in Engineering Management in December, 1972. During the summer of 1964 he worked with American Independent Oil Company in Wafra, Neutral Zone. Upon graduating from the University of Tulsa, he joined the Kuwait Oil Company as a Petroleum Engineer in Ahmadi, Kuwait and remained there until September, 1968. Since then he has been employed by Kuwait University as a staff member on leave of absence. He is a member of Pi Epsilon Tau, National Honor Society of Petroleum Engineers, and Society of Petroleum Engineers of AIME.

APPENDICES

APPENDIX A

NOMENCLATURE

A	=	Cross sectional area normal to the flow direction - cm^2
C	=	Compressibility - atm^{-1}
G	=	Gas flux rate - cc/sec
g	=	Conversion factor of gravity term - .00096714 atm/(gm/cm^2)
h	=	Thickness - cm
I	=	Number of grid elements in r - direction
K	=	Absolute permeability - Darcys
K_g, K_o, K_w	=	Phase effective permeability - Darcys
K_r	=	Relative permeability, fraction
L	=	Number of elemental blocks for dynamic model
M	=	Number of elemental blocks in x - direction
N	=	Number of elemental blocks in y - direction
P	=	Pressure - atm
$\overline{P}$	=	Average pressure - atm
PI	=	Productivity index - cc/sec per atm
PV	=	Pore volume - cc
P_w	=	Producing bottom-hole pressure - atm

P_c = Capillary pressure - atm

q = Production rate - cc/sec

R = Pressure residual - atm

r = Radial distance - cm

r_e = Boundary radius - cm

R_s = Solution gas/oil ratio

R_s' = dR_s/dP - atm^{-1}

r_w = Well radius - cm

S = Saturation - fraction

S_{g_c} = Critical gas saturation - fraction

S_{o_r} = Residual oil saturation - fraction

S_{w_c} = Irreducible water saturation - fraction

T = Transmissibility

t = Time - sec

V = Darcy's velocity (superficial, q/A) - cm/sec

W = Water flux rate - cc/sec

z = Vertical direction - cm, positive downward

Greek Letters:

β = Formation volume factor - res cc/std cc

β' = $d\beta/dP$

ε = Error tolerance

λ = $KhK_r/\mu\beta$ or $KK_r/\mu\beta$

μ	=	Viscosity - cp
ρ	=	Density - gm/cc
Φ	=	Pressure potential - atm
ϕ	=	Porosity - fraction
Δ p	=	Pressure differential - atm
Δ r	=	Width of radial elemental block - cm
Δ t	=	Time increment - sec
Δ x	=	Length of areal elemental block - cm
Δ y	=	Width of areal elemental block - cm

Subscripts:

A	=	Areal model
b	=	Bubble point
g	=	Gas phase
i	=	Indicating ith elemental block in x or r direction
in	=	Input
j	=	Indicating jth elemental block in y- direction
k	=	Indicating the kth elemental block for the dynamic model
o	=	Oil phase
out	=	Output
R	=	Radial model

r	=	Radial direction
s	=	Standard conditions of pressure and temperature (1 atm and 60 degrees F)
T	=	Total
w	=	Water phase

Superscripts:

k	=	Iteration level
n	=	Time level

APPENDIX B

DERIVATION OF THE TWO-DIMENSIONAL THREE-PHASE AREAL MODEL

The areal model developed here is essentially a conventional numerical simulator, which provides for variable grid spacing, variable thickness, and accounts for effects of relative permeability, capillary and gravity forces, reservoir heterogeneity, anisotrophy, and fluid and rock compressibilities.

1. Partial Differential Equations

The concept employed in describing fluid flow in porous media is based on the law of mass conservation:

mass rate in - mass rate out - mass production rate = rate of mass accumulation.....(1A)

and Darcy's law: $V = \frac{K}{\mu} \nabla \Phi$ .....(2A)

Consider three-phase fluid flow through an elemental block in the x and y directions as shown in Figure 1A. Apply the law of mass conservation to each of the three phases:

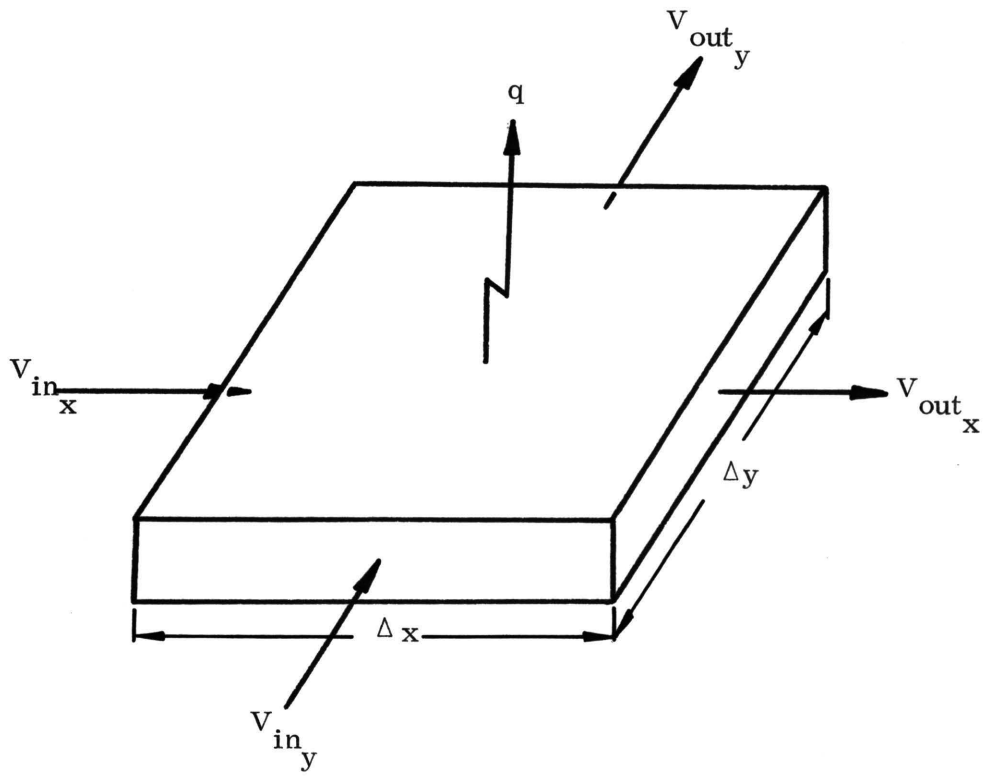

Figure 1A. A Typical Reservoir Elemental Block

Oil phase:

$$\text{mass rate in} = (V_o A \rho_{o_s}/\beta_o)_{in_x} + (V_o A \rho_{o_s}/\beta_o)_{in_y} \quad \text{.............. (3A)}$$

where A is the area normal to the direction of flow; $V_{o_{in_x}}$ and $V_{o_{in_y}}$ are the oil velocities entering the elemental block in the x and y directions, respectively. The oil velocity is defined by Darcy's law as:

$$V_o = -\frac{K_o}{\mu_o} \nabla \Phi_o \quad \text{...................................... (4A)}$$

$$\text{mass rate out} = (V_o A \rho_{o_s}/\beta_o)_{out_x} + (V_o A \rho_{o_s}/\beta_o)_{out_y} \quad \text{............ (5A)}$$

where $V_{o_{out_x}}$ and $V_{o_{out_y}}$ are the oil velocities leaving the elemental block in the x and y directions, respectively. The mass rate out can be defined in terms of the entering mass rates and the change in mass rates within the block as follows:

$$(V_o A \rho_{o_s}/\beta_o)_{out_x} = (V_o A \rho_{o_s}/\beta_o)_{in_x} + \Delta x \frac{\partial}{\partial x}(V_{o_x} A_x \rho_{o_s}/\beta_o)$$

$$\text{.................... (6A)}$$

$$(V_o A \rho_{o_s}/\beta_o)_{out_y} = (V_o A \rho_{o_s}/\beta_o)_{in_y} + \Delta y \frac{\partial}{\partial y}(V_{o_y} A_y \rho_{o_s}/\beta_o)$$

$$\text{The oil mass flow rate} = q_o \rho_{o_s} \quad \text{.................................... (7A)}$$

where q_o is positive for production and negative for injection.

$$\text{Rate of mass accumulation} = h\Delta x \Delta y \rho_{o_s} \frac{\partial}{\partial t}\left(\frac{\phi S_o}{\beta_o}\right) \quad \ldots\ldots\ldots\ldots (8A)$$

In all the above equations ρ_{o_s} is oil density at standard conditions of pressure and temperature (14.65 psi and 60 degrees F), and is therefore constant.

Substituting Equations (3A), (5A), (7A) and (8A) into Equation (1A) and utilizaing the relationships defined by Equations (4A) and (6A), then dividing the resulting equation by $\Delta x \Delta y \rho_{o_s}$ yields:

$$\nabla \cdot (\lambda_o \nabla \Phi_o) - \frac{q_o}{\Delta x \Delta y} = h \frac{\partial}{\partial t}\left(\frac{\phi S_o}{\beta_o}\right) \quad \ldots\ldots\ldots\ldots\ldots\ldots\ldots\ldots (9A)$$

where $\lambda_o = \dfrac{KhK_{r_o}}{\mu_o \beta_o}$ and $K_o = (K)(K_{r_o})$

Expanding the time derivative of Equation (9A), and multiplying both sides of this equation by β_o yields:

$$\beta_o \nabla \cdot (\lambda_o \nabla \Phi_o) - \frac{q_o \beta_o}{\Delta x \Delta y} = h\phi\left[\frac{\partial S_o}{\partial t} + S_o\left(C_r - \frac{1}{\beta_o}\frac{d\beta_o}{dP}\right)\frac{\partial P}{\partial t}\right] \quad \ldots\ldots (10A)$$

where $C_r = \dfrac{1}{\phi}\dfrac{d\phi}{dP}$

Equation (10A) is the partial differential equation describing the flow of oil in two dimensions (x and y directions) in a porous medium.

Water Phase:

Applying logic similar to that employed in deriving the equation for the oil phase, a partial differential equation for the water phase flowing through an elemental block in two dimensions can be developed; it is written as follows:

$$\beta_w \nabla \cdot (\lambda_w \nabla \Phi_w) - \frac{q_w \beta_w}{\Delta x \Delta y} = h \phi \left[\frac{\partial S_w}{\partial t} + S_w (C_r + C_w) \frac{\partial P}{\partial t} \right] \quad \ldots\ldots (11A)$$

where $\lambda_w = \dfrac{KhK_{r_w}}{\mu_w \beta_w}$ and $C_w = -\dfrac{1}{\beta_w} \dfrac{d\beta_w}{dP}$

Gas Phase:

The derivation of the partial differential equation for the gas phase differs from that of the oil and water phases only in that the mass balance must be made on total gas (free gas and gas in solution). The resultant equation can be written as:

$$\nabla \cdot (\lambda_g \nabla \Phi_g) + \nabla \cdot (\lambda_o R_s \nabla \Phi_o) - \left(\frac{q_g + q_o R_s}{\Delta x \Delta y} \right)$$

$$= h \frac{\partial}{\partial t} \left(\frac{\phi S_g}{\beta_g} \right) + h \frac{\partial}{\partial t} \left(\frac{\phi S_o R_s}{\beta_o} \right) \quad \ldots\ldots (12A)$$

where $$\lambda_g = \frac{KhK_{rg}}{\mu_g \beta_g}$$

and q_g refers to production of the free gas phase from the reservoir.

Expanding the time derivative of Equation (12A) yields:

$$h\frac{\partial}{\partial t}\left(\frac{\phi S_g}{\beta_g}\right) + h\frac{\partial}{\partial t}\left(\frac{\phi S_o R_s}{\beta_o}\right) = h\phi\left[\frac{1}{\beta_g}\frac{\partial S_g}{\partial t} + \frac{S_g}{\beta_g}\left(C_r - \frac{1}{\beta_g^2}\frac{d\beta_g}{dP}\right)\right.$$

$$\left.\frac{\partial P}{\partial t}\right] + hR_s\frac{\partial}{\partial t}\left(\frac{\phi S_o}{\beta_o}\right) + h\frac{\phi S_o}{\beta_o}\frac{dR_s}{dP}\frac{\partial P}{\partial t} \quad \text{.....(13A)}$$

Substituting the equivalent of the term $h\frac{\partial}{\partial t}\left(\frac{\phi S_o}{\beta_o}\right)$

from Equation (9A) into Equation (13A) yields:

$$h\frac{\partial}{\partial t}\left(\frac{\phi S_g}{\beta_g}\right) + h\frac{\partial}{\partial t}\left(\frac{\phi S_o R_s}{\beta_o}\right) = h\phi\left\{\frac{1}{\beta_g}\frac{\partial S_g}{\partial t} + \left[\frac{S_g}{\beta_g}\left(C_r - \frac{1}{\beta_g}\frac{d\beta_g}{dP}\right) + \right.\right.$$

$$\left.\left.\frac{S_o}{\beta_o}\frac{dR_s}{dP}\right]\frac{\partial P}{\partial t}\right\} + R_s\nabla\cdot(\lambda_o\nabla\Phi_o) - \frac{q_o R_s}{\Delta x \Delta y} \quad \text{.....(14A)}$$

Substituting the right-hand side of Equation (14A) for the right-hand of Equation (12A), multiplying both sides of the resultant equation by β_g and re-arranging yields:

$$\beta_g \nabla \cdot (\lambda_g \nabla \Phi_g) + \beta_g \nabla \cdot (\lambda_o R_s \nabla \Phi_o) - \beta_g R_s \nabla \cdot (\lambda_o \nabla \Phi_o) - \frac{q_g \beta_g}{\Delta x \Delta y}$$

$$= h \phi \{ \frac{\partial S_g}{\partial t} + [S_g (C_r - \frac{1}{\beta_g} \frac{d\beta_g}{dP}) + \frac{\beta_g}{\beta_o} S_o \frac{dR_s}{dP}] \frac{\partial P}{\partial t} \} \quad \ldots\ldots\ldots (15A)$$

Equation (15A) describes the flow of total gas in two dimensions in a porous medium. Since capillary pressure and gravity forces are accounted for in this model, the following definitions of the potential equations are applicable:

$$\Phi_w = P - P_{c_{ow}} - \rho_w gz$$

$$\Phi_g = P + P_{c_{go}} - \rho_g gz \quad \ldots\ldots\ldots\ldots\ldots\ldots\ldots\ldots\ldots\ldots (16A)$$

and $$\Phi_o = P - \rho_o gz$$

where, $$P \equiv P_o$$

$$P_{c_{ow}} = P_o - P_w$$

$$P_{c_{go}} = P_g + P_o$$

Since the partial differential Equations (10A), (11A) and (15A) are simultaneous equations relating pressure and the three saturations (four dependent variables) to the independent variables, position and time, this system can not be solved as there are three equations and four unknowns. This problem is readily overcome, however, by introducing another equation containing the same dependent variables. This equation is based on the definition of saturations:

$$S_o + S_w + S_g = 1$$

It may be further noted that the partial differential equations have been arranged so that they may be added to yield one equation in one dependent variable (pressure). Note that the three time derivatives of the saturations are isolated so that the sum of the saturation derivatives vanish as follows:

$$\frac{\partial S_o}{\partial t} + \frac{\partial S_w}{\partial t} + \frac{\partial S_g}{\partial t} = 0$$

Summing Equations (10A), (11A) and (15A), re-arranging terms, and simplifying as discussed immediately above, yields:

$$(\beta_o - \beta_g R_s)\nabla \cdot (\lambda_o \nabla \Phi_o) + \beta_w \nabla \cdot (\lambda_w \nabla \Phi_w) + \beta_g \nabla \cdot (\lambda_g \nabla \Phi_g) + \beta_g \nabla \cdot (\lambda_o R_s \nabla \Phi_o)$$

$$-\frac{q_o\beta_o+q_w\beta_w+q_g\beta_g}{\Delta x\ \Delta y} = h\phi\left(C_r+C_wS_w-\frac{S_o}{\beta_o}\beta_o'-\frac{S_g}{\beta_g}\beta_g'+\frac{\beta_g}{\beta_o}S_oR_s'\right)\frac{\partial P}{\partial t} \quad \ldots\ldots\ldots (17A)$$

where $\beta_o' = \frac{d\beta_o}{dP}$

$\beta_g' = \frac{d\beta_g}{dP}$

and $R_s' = \frac{dR_s}{dP}$

Equation (17A) is a non-homogeneous, second-order, non-linear, partial differential equation, and no technique for solving it analytically is known. It is non-linear because the coefficients are pressure and saturation dependent. The equation is solvable, however, by finite difference techniques.

2. Finite Difference Equations

Equation (17A) is in a form which is suitable for conversion to a difference equation from which can be calculated the values of the dependent variables (pressure) at time level t^{n+1}. The terms of the left hand side of Equation (17A) can be represented by a finite difference equation if the time-space region is divided into discrete increments in each direction, then expanded about some point (i, j) in the spatial grid

pattern at some fixed time.

The point at which all parameters are defined in each block is arbitrarily selected as its mid-point. Thus, the center is the focal point at which the pressure is assumed to exist, and this assumption forms the basis for calculating pressure gradients.

Utilizing this convention, Equation (17A) may be written in an implicit difference form as:

$$(\beta_o - \beta_g R_s)^{n+1}_{i,j} (\Delta_x T_o \Delta_x \Phi_o)^{n+1}_{i,j} + \beta^{n+1}_{w_{i,j}} (\Delta_x T_w \Delta_x \Phi_w)^{n+1}_{i,j}$$

$$+ \beta^{n+1}_{g_{i,j}} (\Delta_x T_g \Delta_x \Phi_g)^{n+1}_{i,j} + \beta^{n+1}_{g_{i,j}} (\Delta_x T_o R_s \Delta_x \Phi_o)^{n+1}_{i,j}$$

$$+ (\beta_o - \beta_g R_s)^{n+1}_{i,j} (\Delta_y T_o \Delta_y \Phi_o)^{n+1}_{i,j} + \beta^{n+1}_{w_{i,j}} (\Delta_y T_w \Delta_y \Phi_w)^{n+1}_{i,j}$$

$$+ \beta^{n+1}_{g_{i,j}} (\Delta_y T_g \Delta_y \Phi_g)^{n+1}_{i,j} + \beta^{n+1}_{g_{i,j}} (\Delta_y T_o R_s \Delta_y \Phi_o)^{n+1}_{i,j}$$

$$- QTERM^{n+1}_{i,j} = TRM^{n+1}_{i,j} \Delta_t P \quad \text{.....(18A)}$$

where:

$$\Delta_x T \Delta_x \Phi = T_{i+1/2,j}(\Phi_{i+1,j} - \Phi_{i,j}) - T_{i-1/2,j}(\Phi_{i,j} - \Phi_{i-1,j}),$$

$$T_{i+1/2,j} = \frac{2}{\Delta x_i(\Delta x_{i+1} - \Delta x_i)} \left(\frac{KhK_r}{\mu\beta}\right)_{i+1/2,j},$$

$$T_{i-1/2,j} = \frac{2}{\Delta x_i(\Delta x_i - \Delta x_{i-1})} \left(\frac{KhK_r}{\mu\beta}\right)_{i-1/2,j},$$

$$\Delta_y T \Delta_y \Phi = T_{i,j+1}(\Phi_{i,j+1} - \Phi_{i,j}) - T_{i,j-1/2}(\Phi_{i,j} - \Phi_{i,j-1})$$

$$T_{i,j+1/2} = \frac{2}{\Delta y_j(\Delta y_{j+1} + \Delta y_j)} \left(\frac{KhK_r}{\mu\beta}\right)_{i,j+1/2}$$

$$T_{i,j-1/2} = \frac{2}{\Delta y_j(\Delta y_j + \Delta y_{j-1})} \left(\frac{KhK_r}{\mu\beta}\right)_{i,j-1/2}$$

$$\Delta_t P = P^{n+1} - P^n$$

$$TRM_{i,j} = \frac{(h\phi)_{i,j}}{\Delta t}\left(C_r + C_w S_w - \frac{S_o}{\beta_o}\beta_o' - \frac{S_g}{\beta_g}\beta_g' + \frac{\beta_g}{\beta_o}S_o R_s'\right)_{i,j}$$

$$QTERM_{i,j} = \frac{(q_o\beta_o + q_w\beta_w + q_g\beta_g)_{i,j}}{\Delta x_i \Delta y_j}$$

The terms T_o, T_w and T_g are transmissibility terms for the flows between grid blocks of oil, water, and gas phases, respectively. In addition the term $(T_o R_s)$ is a transmissibility term for the flow, between grid blocks, of solution gas transported in the oil phase. It is noted from Equation (18A) that the pressure and saturation dependent variables have been treated implicitly. Therefore, both the pressure dependent and saturation dependent variables should be evaluated at t^{n+1}. It is also important to use the upstream relative permeability values in Equation (18A), which implies that, dependent on the direction of flow, subscript (i+1/2,j) should be either (i,j) or (i+1,j), and (i-1/2,j) should be either (i,j) or (i-1,j); the same is applicable for y direction. The effective interblock permeability-thickness products, $(Kh)_{i+1/2,j}$, $(Kh)_{i-1/2,j}$, $(Kh)_{i,j+1/2}$, and $(Kh)_{i,j-1/2}$ for x and y directions, respectively, must be evaluated at the interface boundary between the (i,j) grid block and the appropriate adjacent block. The interblock permeability-thickness products are defined as:

$$(Kh)_{i+1/2,j} = \frac{K_{i,j}K_{i+1,j}h_{i+1,j}h_{i,j}(\Delta x_{i+1} + \Delta x_i)}{h_{i+1,j}K_{i+1,j}\Delta x_i + h_{i,j}K_{i,j}\Delta x_{i+1}}$$

$$(Kh)_{i,j+1/2} = \frac{K_{i,j}K_{i,j+1}h_{i,j+1}h_{i,j}(\Delta y_{j+1} + \Delta y_j)}{h_{i,j+1}K_{i,j+1}\Delta y_j + h_{i,j}K_{i,j}\Delta y_{j+1}}$$

Substituting the values of the potential function, defined by Equation (16A), into the difference equation which was formed from the three phase equations, into Equation (18A), and re-arranging yields:

$$AX^{n+1}_{i,j}P^{n+1}_{i-1,j} + (BX_{i,j} + BY_{i,j} - TRM_{i,j})^{n+1}P^{n+1}_{i,j} + CX^{n+1}_{i,j}P^{n+1}_{i+1,j}$$

$$+ AY^{n+1}_{i,j}P^{n+1}_{i,j-1} + CY^{n+1}_{i,j}P^{n+1}_{i,j+1} = E^{n+1}_{i,j} - TRM^{n+1}_{i,j}P^{n}_{i,j} \quad \ldots\ldots\ldots\ldots\ldots (19A)$$

where: $$AX^{n+1}_{i,j} = [\,(\beta_o - \beta_g R_s)_{i,j} T_{o_{i-1/2,j}} +$$

$$\beta_{w_{i,j}} T_{w_{i-1/2,j}} + \beta_{g_{i,j}} T_{g_{i-1/2,j}} + \beta_{g_{i,j}} R_{s_{i-1/2,j}} T_{o_{i-1/2,j}}\,]^{n+1}$$

$$CX_{i,j}^{n+1} = [\,(\beta_o - \beta_g R_s)_{i,j}\, T_{o_{i+1/2,j}} + \beta_{w_{i,j}}\, T_{w_{i+1/2,j}}$$

$$+ \beta_{g_{i,j}}\, T_{g_{i+1/2,j}} + \beta_{g_{i,j}}\, R_{s_{i+1/2,j}}\, T_{o_{i+1/2,j}}\,]^{n+1}$$

$$AY_{i,j}^{n+1} = [\,(\beta_o - \beta_g R_s)_{i,j}\, T_{o_{i,j-1/2}} + \beta_{w_{i,j}}\, T_{w_{i,j-1/2}}$$

$$+ \beta_{g_{i,j}}\, T_{g_{i,j-1/2}} + \beta_{g_{i,j}}\, R_{s_{i,j-1/2}}\, T_{o_{i,j-1/2}}\,]^{n+1}$$

$$CY_{i,j}^{n+1} = [\,(\beta_o - \beta_g R_s)_{i,j}\, T_{o_{i,j+1/2}} + \beta_{w_{i,j}}\, T_{w_{i,j+1/2}}$$

$$+ \beta_{g_{i,j}}\, T_{g_{i,j+1/2}} + \beta_{g_{i,j}}\, R_{s_{i,j+1/2}}\, T_{o_{i,j+1/2}}\,]^{n+1}$$

$$BX_{i,j}^{n+1} = -AX_{i,j}^{n+1} - CX_{i,j}^{n+1}$$

$$BY_{i,j}^{n+1} = -AY_{i,j}^{n+1} - CY_{i,j}^{n+1}$$

$$E_{i,j}^{n+1} = QTERM_{i,j}^{n+1} + PCTRM_{i,j}^{n+1} + GTRM_{i,j}^{n+1}$$

$$PCTRM_{i,j}^{n+1} = \beta_{w_{i,j}}^{n+1} \left(\Delta_x T_w \Delta_x P_{c_{ow}} \right)_{i,j}^{n+1}$$

$$+ \beta_{w_{i,j}}^{n+1} \left(\Delta_y T_w \Delta_y P_{c_{ow}} \right)_{i,j}^{n+1}$$

$$- \beta_{g_{i,j}}^{n+1} \left(\Delta_x T_g \Delta_x P_{c_{go}} \right)_{i,j}^{n+1}$$

$$- \beta_{g_{i,j}}^{n+1} \left(\Delta_y T_g \Delta_y P_{c_{go}} \right)_{i,j}^{n+1}$$

$$GTRM_{i,j}^{n+1} = \left(\beta_o - \beta_g R_s\right)_{i,j}^{n+1} \left[\Delta_x T_o \Delta_x (\rho_o gz) \right]_{i,j}^{n+1} +$$

$$\beta_{w_{i,j}}^{n+1} \left[\Delta_x T_w \Delta_x (\rho_w gz) \right]_{i,j}^{n+1} + \beta_{g_{i,j}}^{n+1} \left[\Delta_x T_g \Delta_x (\rho_g gz) \right]_{i,j}^{n+1}$$

$$+ \beta_{g_{i,j}}^{n+1} \left[\Delta_x T_o R_s \Delta_x (\rho_o gz) \right]_{i,j}^{n+1} + \left(\beta_o - \beta_g R_s\right)_{i,j}$$

$$[\Delta_y T_o \Delta_y (\rho_o gz)]^{n+1}_{i,j} + \beta^{n+1}_{w_{i,j}} [\Delta_y T_w \Delta_y (\rho_w gz)]^{n+1}_{i,j}$$

$$+ \beta^{n+1}_{g_{i,j}} [\Delta_y T_g \Delta_y (\rho_g gz)]^{n+1}_{i,j} + \beta^{n+1}_{g_{i,j}} [\Delta_y T_o R_s \Delta_y (\rho_o gz)]^{n+1}_{i,j}$$

Equation (19A), written about each point in the grid, forms a set of simultaneous equations which can be solved by numerical techniques. In matrix notation, the resulting set of equations may be written

$$A\overline{P} = \overline{D}$$

where $\overline{P}$ is the solution vector, $\overline{D}$ is the vector of known parameters and A is an $(MxN)^2$ penta-diagonal matrix of coefficients. Since the implicit coefficients are known, the system may be solved as a set of linear equations. A solution was obtained in this study using a combination of the Alternating Direction Implicit (ADI) procedure and the Pressure Residual Relaxation Method.

3. Solution of the Areal Numerical Simulator - Combination of Alternating Direction Implicit Procedure (ADI) and Pressure Residual Relaxation Method

To illustrate the ADI method, Equation (19A) can be written implicitly in P as:

$$AX_{i,j}^{n+1} P_{i-1,j}^{2k+1,n+1} + BX_{i,j}^{n+1} P_{i,j}^{2k+1,n+1} + CX_{i,j}^{n+1} P_{i+1,j}^{2k+1,n+1}$$

$$+ AY_{i,j}^{n+1} P_{i,j-1}^{2k,n+1} + BY_{i,j}^{n+1} P_{i,j}^{2k,n+1} + CY_{i,j}^{n+1} P_{i,j+1}^{2k,n+1}$$

$$= 2.(HK)TRM_{i,j}^{n+1}(P_{i,j}^{2k+1,n+1} - P_{i,j}^{2k,n+1}) + E_{i,j}^{n+1} \quad \text{.....(20A)}$$

where HK is the iteration parameter which depends on the grid size used; it is selected according to the method suggested by Welge and Weber.[7] $P_{i,j+1}^{2k,n+1}$, $P_{i,j}^{2k,n+1}$ and $P_{i,j-1}^{2k,n+1}$ are the values of P obtained from the previous half iteration in the y - direction (j); they are held constant during the (2k+1)th iteration in the x - direction (i). Also note that Δt is halved; therefore $TRM_{i,j}$ in the right hand side of Equation (20A) is multiplied by 2 since Δt appears in the denominator of $TRM_{i,j}$. Equation (20A) is implicit in the x - direction (i) with three unknowns, $P_{i-1,j}^{2k+1,n+1}$, $P_{i,j}^{2k+1,n+1}$ and $P_{i+1,j}^{2k+1,n+1}$. An equation identical to Equation (20A) but with each superscript k increased by 1, would be implicit in the y - direction (j) with unknowns, $P_{i,j-1}^{2k+2,n+1}$, $P_{i,j}^{2k+2,n+1}$ and $P_{i,j+1}^{2k+2,n+1}$ and the P's with superscripts 2k+1 held constant. Thus the solution of Equation (20A) is comprised of two parts, obtained by iterating in the x - direction a row at a time, then holding these values constant and iterating in the

y - direction a column at a time.

It may be observed that Equation (20A) represents a set of linear equations each having three unknowns. Each row and each column in the model's grid system would yield such a set of linear equations, containing as many equations as there are mesh points in the row or the column. Thus, for each row, or column, a tri-diagonal matrix would be formed. Gaussian Elimination provides a very efficient solution of such a matrix. A complete sweep through every row and every column comprises an iteration. Iterations (for the same time step) are continued until the difference between the answers from two successive iterations for P, iterated one at a time, does not exceed the desired error tolerance. If convergence is not achieved in one complete iteration, another iteration parameter is selected and the iteration is repeated using the value of P computed in the previous iteration.

In the present work, one complete iteration was performed by setting the iteration parameter HK equal to unity, then the pressure residuals were relaxed untilthe largest normalized pressure residual did not exceed the desired error tolerance. The normalized pressure residual is defined as:

$$R^{k}_{i,j} = (AX^{n+1}_{i,j} P^{n+1,k}_{i-1,j} + CX^{n+1}_{i,j} P^{n+1,k}_{i+1,j} + AY^{n+1}_{i,j} P^{n+1,k}_{i,j-1}$$

$$+ CY_{i,j}^{n+1} P_{i,j+1}^{n+1,k} - E_{i,j}^{n+1} + TRM_{i,j}^{n+1} P_{i,j}^{n})/F + P_{i,j}^{n+1,k} \quad \text{.....(21A)}$$

where $$F = BX_{i,j}^{n+1} + BY_{i,j}^{n+1} - TRM_{i,j}^{n+1}$$

Convergence is obtained in the relaxation method used here by forcing the residual of Equation (21A) to zero by correcting $P_{i,j}^{n+1,k}$ as follows:

$$P_{i,j}^{n+1,k+1} = P_{i,j}^{n+1,k} - R_{i,j}^{k} \quad \text{.....(22A)}$$

so that $R_{i,j}^{k+1} = 0.$

This correction of $R_{i,j}^{k}$ to zero requires that the residuals in the adjacent elemental blocks, (i-1, j), (i+1, j), (i, j-1) and (i, j+1) be corrected. The procedure used is demonstrated as follows by correcting the residual at the (i-1, j) location. The definition of this residual, before correcting is

$$R_{i-1,j}^{k} = \frac{1}{F_{i-1,j}} (AX_{i-1,j}^{n+1} P_{i-2,j}^{n+1,k+1} + CX_{i-1,j}^{n+1} P_{i,j}^{n+1,k} + AY_{i-1,j}^{n+1}$$

$$P_{i-1,j-1}^{n+1,k+1} + CY_{i-1,j}^{n+1} P_{i-1,j+1}^{n+1,k} - E_{i-1,j}^{n+1} + TRM_{i-1,j}^{n+1}$$

$$P^{n}_{i-1,j} + F_{i-1,j} P^{n+1,k+1}_{i-1,j}) \quad \text{.....(23A)}$$

$$R^{k+1}_{i-1,j} = \frac{1}{F_{i-1,j}} (AX^{n+1}_{i-1,j} P^{n+1,k+1}_{i-2,j} + CX_{i-1,j} P^{n+1,k+1}_{i,j}$$

$$+ AY^{n+1}_{i-1,j} P^{n+1,k+1}_{i-1,j-1} + CY^{n+1}_{i-1,j} P^{n+1,k}_{i-1,j+1} - E^{n+1}_{i-1,j}$$

$$+ TRM^{n+1}_{i-1,j} P^{n}_{i-1,j} + F_{i-1,j} P^{n+1,k+1}_{i-1,j}) \quad \text{.....(24A)}$$

Subtracting Equation (23A) from Equation (24A) yields:

$$R^{k+1}_{i-1,j} - R^{k}_{i-1,j} = \frac{CX^{n+1}_{i-1,j}}{F_{i-1,j}} (P^{n+1,k+1}_{i,j} - P^{n+1,k}_{i,j}) \quad \text{.....(25A)}$$

but $R^{k}_{i,j} = P^{n+1,k}_{i,j} - P^{n+1,k+1}_{i,j}$ from Equation (22A);

therefore $$R^{k+1}_{i-1,j} = R^{k}_{i-1,j} - \frac{CX^{n+1}_{i-1,j}}{F_{i-1,j}} R^{k}_{i,j} \quad \text{.....(26A)}$$

Similarly,
$$R^{k+1}_{i+1,j} = R^{k}_{i+1,j} - \frac{AX^{n+1}_{i+1,j}}{F_{i+1,j}} R^{k}_{i,j} \quad \text{.....(27A)}$$

$$R^{k+1}_{i,j-1} = R^{k}_{i,j-1} - \frac{CY^{n+1}_{i,j-1}}{F_{i,j-1}} R^{k}_{i,j} \quad \text{.....(28A)}$$

and
$$R^{k+1}_{i,j+1} = R^{k}_{i,j+1} - \frac{AY^{n+1}_{i,j+1}}{F_{i,j+1}} R^{k}_{i,j} \quad \text{.....(29A)}$$

The calculation scheme is as follows:

a. Calculate $R^{k}_{i,j}$ by Equation (21A) using the calculated pressures from ADI.

b. Correct the pressure of the elemental block, $P^{n+1,k}_{i,j}$, using Equation (22A).

c. Correct the pressure residuals for the blocks adjacent to elemental block (i,j) using Equations (26A) through (29A).

d. Set $R^{k+1}_{i,j} = 0.0$.

e. Repeat steps b through d for the rest of the elemental blocks.

f. Terminate the iterative procedure when the maximum pressure residual does not exceed specified tolerance.

It was found that this method converged more rapidly than iterative ADI, thus reducing computational time and obtaining a more accurate determination of the fluid saturations. The combination of the (ADI) and the pressure residual relaxation methods is competitive with any other available technique.

4. <u>Material Balance Solution</u>

Each phase saturation may be calculated explicitly for each block after expanding Equations (10A), (11A) and (15A) as finite difference equations. The result of this expansion follows for each phase.

Oil phase saturation:

Equation (10A) written in a finite difference form yields:

$$\beta_{o_{i,j}}^{n+1} (\Delta_x T_o \Delta_x \Phi_o)_{i,j}^{n+1} + \beta_{o_{i,j}}^{n+1} (\Delta_y T_o \Delta_y \Phi_o)_{i,j}^{n+1} -$$

$$\frac{(q_o \beta_o)_{i,j}^{n+1}}{\Delta x_i \Delta y_j} = \frac{\phi_{i,j}^{n+1} h_{i,j}}{\Delta t} [(S_{o_{i,j}}^{n+1} - S_{o_{i,j}}^{n}) + S_{o_{i,j}}^{n+1}$$

$$(C_r - \frac{1}{\beta_o} \beta_o')_{i,j}^{n+1} \Delta_t P] \quad \ldots\ldots\ldots\ldots\ldots\ldots\ldots\ldots\ldots\ldots\ldots (30A)$$

Equation (30A) is rearranged and solved for $S_{o_{i,j}}^{n+1}$,

$$S_{o_{i,j}}^{n+1} = (AOMX_{i,j}^{n+1} + AOMY_{i,j}^{n+1} - QOT_{i,j}^{n+1} + S_{o_{i,j}}^{n})/COMPRO_{i,j}^{n+1} \quad \ldots (31A)$$

where $$AOMX_{i,j}^{n+1} = ZO(\Delta_x T_o \Delta_x \Phi_o)_{i,j}^{n+1}$$

$$AOMY_{i,j}^{n+1} = ZO(\Delta_y T_o \Delta_y \Phi_o)_{i,j}^{n+1}$$

$$QOT_{i,j}^{n+1} = ZO\left(\frac{q_{o_{i,j}}^{n+1} \beta_{o_{i,j}}}{\Delta x_i \, \Delta y_i}\right)$$

$$ZO = \frac{\Delta t \beta_{o_{i,j}}^{n+1}}{\phi_{i,j}^{n+1} h_{i,j}}$$

$$COMPRO_{i,j}^{n+1} = \left[1 + \left(C_r - \frac{1}{\beta_{o_{i,j}}^{n+1}} \beta_{o_{i,j}}^{'n+1}\right) \Delta_t P\right]$$

Water phase saturation:

Equation (11A) written in a finite difference form yields a result which is identical to Equation (31A), except for the phase subscript. It is given below.

$$S_{w_{i,j}}^{n+1} = (AWMX_{i,j}^{n+1} + AWMY_{i,j}^{n+1} - QWT_{i,j}^{n+1} + S_{w_{i,j}}^{n})/COMPRW_{i,j}^{n+1} \quad \ldots . (32A)$$

where $$AWMX_{i,j}^{n+1} = ZW(\Delta_x T_w \Delta_x \Phi_w)_{i,j}^{n+1}$$

$$AWMY_{i,j}^{n+1} = ZW(\Delta_y T_w \Delta_y \Phi_w)_{i,j}^{n+1}$$

$$QWT_{i,j}^{n+1} = ZW\left(\frac{q_w \beta_w}{\Delta x_i \Delta y_j}\right)_{i,j}^{n+1}$$

$$ZW = \frac{\Delta t \beta_{w_{i,j}}^{n+1}}{\phi_{i,j}^{n+1} h_{i,j}}$$

$$COMPRW_{i,j}^{n+1} = [\ 1 + (C_r + C_w)\Delta_t P\ ]$$

Gas Phase Saturation:

Expanding Equation (15A) in a finite difference form yields:

$$S_{g_{i,j}}^{n+1} = (AGMX_{i,j}^{n+1} + AGMY_{i,j}^{n+1} + ASGMX_{i,j}^{n+1} + ASGMY_{i,j}^{n+1}$$

$$- QGT_{i,j}^{n+1} - RST_{i,j}^{n+1} + S_{g_{i,j}}^{n})/COMPRG_{i,j}^{n+1} \quad \ldots\ldots\ldots\ldots\ldots (33A)$$

where $$AGMX_{i,j}^{n+1} = ZG(\Delta_x T_g \Delta_x \Phi_g)_{i,j}^{n+1}$$

$$AGMY_{i,j}^{n+1} = ZG(\Delta_y T_g \Delta_y \Phi_g)_{i,j}^{n+1}$$

$$ASGMX_{i,j}^{n+1} = ZG(\Delta_x R_s T_o \Delta_x \Phi_o) - ZG(R_s)(\Delta_x T_o \Delta_x \Phi_o)$$

$$ASGMY_{i,j}^{n+1} = ZG(\Delta_y R_s T_o \Delta_y \Phi_o) - ZG(R_s)(\Delta_y T_o \Delta_y \Phi_o)$$

$$QGT_{i,j}^{n+1} = ZG(\frac{q_g \beta_g}{\Delta x \, \Delta y})_{i,j}^{n+1}$$

$$ZG = \frac{\Delta t \beta_{g_{i,j}}^{n+1}}{\phi_{i,j}^{n+1} h_{i,j}}$$

$$RST_{i,j}^{n+1} = \left(\frac{S_o \beta_g}{\beta_o} R_s'\right)_{i,j}^{n+1} \Delta_t P$$

$$COMPRG_{i,j}^{n+1} = \left[1 + \left(C_r - \frac{1}{\beta_{g_{i,j}}^{n+1}} \beta_{g_{i,j}}'^{n+1}\right) \Delta_t P \right]$$

APPENDIX C

DERIVATION OF THE ONE-DIMENSIONAL, THREE-PHASE RADIAL MODEL

The derivation of the mathematical relationships for radial flow of oil, water and gas in porous media is similar to that for the areal model. The only differences are the value of the area normal to the direction of fluid flow and in the calculation of pore volume. The area for the radial model is calculated as

$$A_r = 2\pi rh \qquad (34A)$$

The pore volume calculation appears in the rate of mass accumulation term, [Equation (7A)] for the areal model. For the radial model it is

$$\pi(r^2_{i+1/2} - r^2_{i-1/2})h\rho_s \frac{\partial}{\partial t}\left(\frac{\phi S}{\beta}\right) \qquad (35A)$$

where $r_{i+1/2}$ and $r_{i-1/2}$ are boundary radii of the radial cell, and r_i is the centered radius of the radial cell i. Therefore, Equation (35A) can be written as

$$2\pi r_i \Delta r_i h \rho_s \frac{\partial}{\partial t}\left(\frac{\phi S}{\beta}\right) \quad \text{.....(36A)}$$

where $\Delta r_i = r_{i+1/2} - r_{i-1/2}$

1. Partial Differential Equations

Following an identical procedure as in the areal model, a partial differential equation for each phase can be derived. Summing the three equations for the phases (oil, water and gas) yields:

$$\frac{1}{r}(\beta_o - \beta_g R_s)\frac{\partial}{\partial r}\left(r \lambda_{o_r} \frac{\partial \Phi_o}{\partial r}\right) + \frac{1}{r}\beta_w \frac{\partial}{\partial r}\left(r \lambda_{w_r} \frac{\partial \Phi_w}{\partial r}\right)$$

$$+ \frac{1}{r}\beta_g \frac{\partial}{\partial r}\left(r \lambda_{g_r} \frac{\partial \Phi_g}{\partial r}\right) + \frac{1}{r}\beta_g \frac{\partial}{\partial r}\left(r R_s \lambda_{o_r} \frac{\partial \Phi_o}{\partial r}\right)$$

$$- \frac{(\beta_o q_o + \beta_w q_w + \beta_g q_g)}{2\pi r \Delta r h} = \phi\left(C_r + S_w C_w - \frac{S_o \beta_o'}{\beta_o} - \frac{S_g \beta_g'}{\beta_g}\right.$$

$$\left. + \frac{\beta_g S_o R_s'}{\beta_o}\right) \frac{\partial P}{\partial t} \quad \text{.....(37A)}$$

where $\lambda_r = \frac{KK_r}{\mu\beta}$

2. Finite Difference Equations

Equation (37A) can be written as a difference equation similar to that for the areal model. A complete solution of Equation (37A) in difference form is:

$$\frac{1}{r_i}[(\beta_o - \beta_g R_s)_i^{n+1} (\Delta_r T_{o_r} \Delta_r \Phi_o)_i^{n+1} + \beta_{w_i}^{n+1} (\Delta_r T_{w_r} \Delta_r \Phi_w)_i^{n+1}$$

$$+ \beta_{g_i}^{n+1} (\Delta_r T_{g_r} \Delta_r \Phi_g)_i^{n+1} + \beta_{g_i}^{n+1} (\Delta_r R_s T_{o_r} \Delta_r \Phi_o)_i^{n+1}]$$

$$- QTERM_i^{n+1} = TR_i^{n+1} \Delta_t P \quad \text{.....(38A)}$$

where:

$$\Delta_r T_r \Delta_r \Phi = T_{r_{i+1/2}} (\Phi_{i+1} - \Phi_i) - T_{r_{i-1/2}} (\Phi_i - \Phi_{i-1})$$

$$T_{r_{i+1/2}} = \frac{1}{\Delta r_i \ln(\frac{r_{i+1}}{r_i})} \left[\frac{(K)(K_r)}{\mu \beta} \right]_{i+1/2}$$

$$T_{r_{i-1/2}} = \frac{1}{\Delta r_i \ln(\frac{r_i}{r_{i-1}})} \left[\frac{(K)(K_r)}{\mu \beta} \right]_{i-1/2}$$

$$TR_i^{n+1} = \frac{\phi_i}{\Delta t}\left[C_r + S_w C_w - \frac{S_o}{\beta_o}\beta_o' - \frac{S_g}{\beta_g}\beta_g' + \frac{\beta_g S_o R_s'}{\beta_o}\right]$$

$$QTERM_{i,j}^{n+1} = \frac{(q_o\beta_o + q_w\beta_w + q_g\beta_g)_i^{n+1}}{2\pi r_i \Delta r_i h_i}$$

The effective interblock permeabilities $K_{i+1/2}$ and $K_{i-1/2}$ are series averaged permeabilities between i and i+1, and i and i-1, respectively.

Since the radial model is horizontal, gravity forces are neglected; therefore the potential functions may be written as follows:

$$\Phi_o = P_o \equiv P$$

$$\Phi_w = P_w = P - P_{c_{ow}} \qquad \text{.....(39A)}$$

$$\Phi_g = P_g = P + P_{c_{go}}$$

Collecting terms associated with P_{i-1}, P_i and P_{i+1} in Equation (38A) respectively, will yield the following equation

$$AR_i^{n+1}P_{i-1}^{n+1} + BR_i^{n+1}P_i^{n+1} + CR_i^{n+1}P_{i+1}^{n+1} = D_i^{n+1} \qquad \text{.....(40A)}$$

where:

$$AR_i^{n+1} = \frac{1}{r_i} \left[(\beta_o - \beta_g R_s)_i T_{o_{ri-1/2}} + \beta_{w_i} T_{w_{ri-1/2}} \right.$$

$$\left. + \beta_{g_i} T_{g_{ri-1/2}} + \beta_{g_i} R_{s_{i-1/2}} T_{o_{ri-1/2}} \right]^{n+1}$$

$$CR_i^{n+1} = \frac{1}{r_i} \left[(\beta_o - \beta_g R_s)_i T_{o_{ri+1/2}} + \beta_{w_i} T_{w_{ri+1/2}} \right.$$

$$\left. + \beta_{g_i} T_{g_{ri+1/2}} + \beta_{g_i} R_{s_{i+1/2}} T_{o_{ri+1/2}} \right]^{n+1}$$

$$BR_i^{n+1} = -AR_i^{n+1} - CR_i^{n+1} - TR_i^{n+1}$$

$$D_i^{n+1} = QTERM_i^{n+1} + PCTRM_i^{n+1} - TR_i^{n+1} P_i^n$$

$$PCTRM_i^{n+1} = \frac{1}{r_i} \left[\beta_{w_i}^{n+1} \left(\Delta_r T_{w_r} \Delta_r P_{c_{ow}} \right)_i^{n+1} \right.$$

$$- \beta_{g_i}^{n+1} \left(\Delta_r T_{g_r} \Delta_r P_{c_{go}} \right)_i^{n+1}]$$

Equation (40A) is a set of simultaneous equations containing as many equations as there are grid elements. Application of appropriate boundary conditions reduces the number of unknowns to the number of equations. Thus, a tri-diagonal coefficient matrix is formed.

3. Material Balance Solution

The material balance solution follows the same procedure discussed for the areal model.

4. Effective Interblock Permeabilities Determination ($K_{i+1/2}$ and $K_{i-1/2}$) by Series Averaging

The derivation of $K_{i+1/2}$ and $K_{i-1/2}$ are based on an assumption of steady-state, by assuming the rate of flow q to be constant for the radial cells i, i+1 and i-1. The total pressure drop between radial cells i+1 and i-1 is equal to sum of incremental cell pressure drops. The grid system is illustrated by Figure 2A. The following derivation shows the proper relationship for calculating $K_{i+1/2}$:

$$\Delta P_T = \Delta P_i + \Delta P_{i+1} \quad \text{.....(41A)}$$

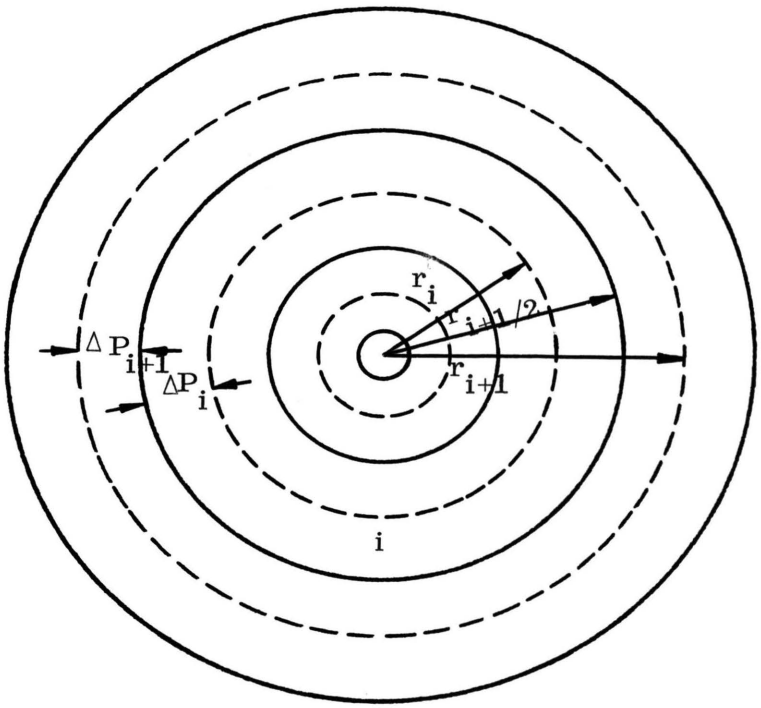

Figure 2A. Illustration of Series-Averaging Technique for Permeabilities

$$q_T = q_i = q_{i+1}$$

$$q_i = \frac{2\pi K_i h_i}{\mu \ln\left(\frac{r_{i+1/2}}{r_i}\right)} \Delta P_i \quad \text{.....(42A)}$$

$$q_{i+1} = \frac{2\pi K_{i+1} h_i}{\mu \ln\left(\frac{r_{i+1}}{r_{i+1/2}}\right)} \Delta P_{i+1} \quad \text{.....(43A)}$$

$$q_T = \frac{2\pi \bar{K} h_i}{\mu \ln\left(\frac{r_{i+1}}{r_i}\right)} \Delta P_T \quad \text{.....(44A)}$$

From Equation (42A),

$$\Delta P_i = \frac{q_i \mu \ln\left(\frac{r_{i+1/2}}{r_i}\right)}{2\pi K_i h_i} \quad \text{.....(45A)}$$

and from Equation (43A)

$$\Delta P_{i+1} = \frac{q_{i+1} \mu \ln\left(\frac{r_{i+1}}{r_{i+1/2}}\right)}{2\pi K_{i+1} h_i} \quad \text{.....(46A)}$$

and from Equation (44A)

$$\Delta P_T = \frac{q_T \mu \ln\left(\frac{r_{i+1}}{r_i}\right)}{2\pi \overline{K} h_i} \quad \text{.......(47A)}$$

Substituting Equations (45A), (46A) and (47A) into Equation (41A) yields:

$$\frac{\ln\left(\frac{r_{i+1}}{r_i}\right)}{\overline{K}} = \frac{\ln\left(\frac{r_{i+1/2}}{r_i}\right)}{K_i} + \frac{\ln\left(\frac{r_{i+1}}{r_{i+1/2}}\right)}{K_{i+1}} \quad \text{.......(48A)}$$

Solving Equation (48A) for $\overline{K}$ yields,

$$\overline{K} = K_{i+1/2} = \frac{K_i K_{i+1} \ln\left(\frac{r_{i+1}}{r_i}\right)}{K_{i+1} \ln\left(\frac{r_{i+1/2}}{r_i}\right) + K_i \ln\left(\frac{r_{i+1}}{r_{i+1/2}}\right)} \quad \text{.......(49A)}$$

Similarly,

$$K_{i-1/2} = \frac{K_i K_{i-1} \ln\left(\frac{r_i}{r_{i-1}}\right)}{K_i \ln\left(\frac{r_{i-1/2}}{r_{i-1}}\right) + K_{i+1} \ln\left(\frac{r_i}{r_{i+1/2}}\right)} \quad \text{.......(50A)}$$

APPENDIX D

NEW TECHNIQUE FOR SATURATION CALCULATION (DYNAMIC APPROACH)

The dynamic material balance technique is based on a new concept for calculating saturations based on net flux in a cell. The new approach calculates the correct material balance and includes a method of calculating the saturations necessary to maintain this balance under current flowing conditions in the model. This was accomplished by establishing directly all terms in the material balance except the rate of production, then computing the rate. The balance was made on the gas phase in this work and this is related to the oil rate by the ratio of mobilities of oil and gas. This ratio is uniquely related to saturations and can be used to calculate the correct saturations with two mobile phases.

The grid system used is illustrated by Figure 6 in Chapter IV. The technique described above can be stated quantitatively for the gas phase by the following equation:

$$X1 = X2 + X3 - X4 \quad \text{.....(51A)}$$

where,

X1 = Total gas mass production rate, gm/sec; the use of expression "total gas" in this work implies that free gas and solution gas are both accounted for.

X2 = Mass rate of total gas influx, gm/sec, into the outer boundary of the dynamic model, calculated from the standard radial model which is interfaced with the dynamic model.

X3 = Total gas present in the dynamic model at the old time, t^n, divided by the time step, Δt; gm/sec.

X4 = Same as X3, except it is evaluated at the "new" time level, t^{n+1}.

Equation (51A), expressed mathematically for the gas phase, is:

$$\left(q_o \frac{K_g}{K_o} \frac{\mu_o \beta_o}{\mu_g \beta_g}\right)_i^{n+1} + q_{o_i}^{n+1} R_{s_i}^{n+1} = G_{in}^{n+1} + \frac{1}{\Delta t} \sum_{k=i}^{L} \left[PV_k \left(\frac{S_g}{\beta_g} + \frac{S_o R_s}{\beta_o}\right) \right]_k^n - \frac{1}{\Delta t} \sum_{k=i}^{L} \left[PV_k \left(\frac{S_g}{\beta_g} + \frac{S_o R_s}{\beta_o}\right) \right]_k^{n+1} \quad \text{.....(52A)}$$

$$i = 1, 2, \ldots, L$$

where $$PV = 2\pi r \Delta r h \phi \quad \ldots\ldots\ldots\ldots\ldots\ldots\ldots\ldots\ldots\ldots (53A)$$

and G_{in} is the total gas influx at the outer boundary of the dynamic model; it is calculated from the conventional radial model using the following equation:

$$G_{in}^{n+1} = 2\pi (T_g)^{n+1}_{r_{L+1/2}} (\Phi_{g_{L+1}} - \Phi_{g_L})^{n+1} + 2\pi (T_{o_r} R_s)_{L+1/2} (\Phi_{o_{L+1}} - \Phi_{o_L})^{n+1}$$

$$\ldots\ldots\ldots\ldots\ldots\ldots\ldots\ldots (54A)$$

It should be noted that all the terms in Equation (54A) are known since the pressures at the new time level, t^{n+1}, have already been computed from the conventional radial model. The gas and oil relative permeabilities in the terms, T_{g_r} and T_{o_r}, are evaluated from upstream saturation values.

Equation (52A) is the same as the mass balance indicated by Equation (51A) since density, which is calculated at standard conditions of temperature and pressure and is constant, is cancelled from each term.

Solving Equation (52A) for $(K_g/K_o)^{n+1}_i$ yields,

$$\left(\frac{K_g}{K_o}\right)^{n+1}_i = \left\{ G_{in}^{n+1} + \frac{1}{\Delta t} \sum_{k=i}^{L} \left[PV_k \left(\frac{S_g}{\beta_g} + \frac{S_o R_s}{\beta_o} \right) \right]_k^n \right.$$

$$- \frac{1}{\Delta t} \sum_{k=i}^{L} \left[PV_k \left(\frac{S_g}{\beta_g} + \frac{S_o R_s}{\beta_o} \right) \right]_k^{n+1}$$

$$\left. - q_{o_i}^{n+1} R_{s_i}^{n+1} \right\} \left(\frac{\mu_g \beta_g}{q_o \mu_o \beta_o} \right)_i^{n+1} \qquad \text{.....(55A)}$$

Since the relative permeability ratio is a function of gas saturation $(K_g/K_o) = f(S_g)$, $S_{g_i}^{n+1}$ is computed from this relationship. This ratio (K_g/K_o) is a unique function of gas saturation since the case treated here does not contain mobile water. The relationship would become more complex if three mobile phases were present.

The approach described by Equation (55A) is an iterative one by nature since one of the "known" values is gas saturation at the new time level. However, in the small cells where these saturations change rapidly, the pore volume is so small that errors in these quantities $(S_{g_i}^{n+1})$ are not significant and are lost in machine round-off errors. Therefore, the method converges rapidly. It may be noted that this same round-off error causes the conventional method to become unstable.

Another possible problem which may be noted is that Equation (55A) has no meaning during the period when a cell has dropped below the bubble-point pressure but has not built up a mobile gas saturation. This is avoided by reverting to a standard oil balance when this occurs. Again, round-off error in the small blocks could cause stability problems with the oil balance. As expected, however, this transition, from zero saturation to mobile gas saturation, in the small cells near the well bore occurs very rapidly and the problem did not appear in this work. The reason this transition occurs so rapidly is that many pore volumes flow through the small cells during a time step. Therefore, they act more as separators than as "material balance" entities during the dynamic calculations.

Although the case of water blockage was not studied in this work, it may be noted that the approach is identical to that for gas. The equation for computing water saturation is given as follows:

$$\left(\frac{K_w}{K_o}\right)^{n+1}_i = \left[W_{in} + \frac{1}{\Delta t} \sum_{k=i}^{L} \left(\frac{PVS_w}{\beta_w}\right)^n_k - \frac{1}{\Delta t} \sum_{k=i}^{L} \left(\frac{PVS_w}{\beta_w}\right)^{n+1}_k \right]$$

$$\left(\frac{\mu_w \beta_w}{q_o \mu_o \beta_o}\right)^{n+1}_i \qquad \text{(56A)}$$

$$i = 1,2,\ldots,L$$

where W_{in} is the water influx into the outer boundary of the dynamic model from the conventional radial model and is calculated using the following equation:

$$W_{in}^{n+1} = 2\pi(T_{w_r})_{L+1/2}^{n+1} \left(\Phi_{w_{L+1}} - \Phi_{w_L} \right)^{n+1} \quad \text{.....(57A)}$$

$S_{w_i}^{n+1}$ is calculated from K_w/K_o relationship.

The previous discussion relating to the gas phase also applies to the water Equations (56A) and (57A).

The oil phase saturation is calculated from the following equation:

$$S_{o_i}^{n+1} = 1.0 - S_{w_i}^{n+1} - S_{g_i}^{n+1} \quad \text{.....(58A)}$$

This completes the calculation by the dynamic material balance approach. Oil saturation calculated by Equation (58A) is accurate since the material balance errors are minimal. Although it is not treated in this work, the principal criterion which assures that the saturations will sum to unity is that the material balance calculations be accurate.

APPENDIX E

COMPUTATIONAL DATA

Number of grid points in reservoir model, (MxN) = 10 x 10.

Grid length Δx = 528 feet*

Grid width Δy = 528 feet

Number of grid elements in radial well simulator, I = 14. The dimensions are as follows:

Block Centered Radii in Feet

0.81	2.40	7.03	20.60	60.36
101.55	124.66	147.77	170.88	193.98
217.09	240.20	263.31	286.41	

r_w = .416 feet

---

* Units in this section are as defined. In the Nomenclature (Appendix A) the units are noted in cgs since that system was used in equations. Data are customarily read into a computer program in English units and converted internally into cgs.

Number of grid elements for the dynamic model: L = 5. The dimensions are as follows:

Block Centered Radii in Feet

0.82	2.40	7.03	20.60	60.36

Permeability k = 50 md.

Porosity ϕ = 20%

Irreducible water saturation S_{w_c} = 18%

Residual oil saturation, S_{o_r} = 18%

Equilibrium gas saturation, S_{g_c} = 5%

Initial reservoir pressure at -6130 feet = 2855 psi

Bubble point pressure, P_b = 2173 psi

Oil formation volume factor at P_b, β_{o_b} = 1.4437

Oil viscosity at P_b, μ_{o_b} = 1.0467 cp

Oil density at P_b, ρ_{o_b} = 39.4726 lb/ft^3

Initial gas saturation = 0.0%

Initial solution gas, R_{s_b} = 573 scf/bbl

Reservoir pore volume = 19.86 million bbl

Initial oil in place = 8.027 million bbl

Natural water influx = None

Allowable oil production rate = 197 bbl/day per well

Oil compressibility, $C_o = 1.5 \times 10^{-5}$ psi^{-1}

Water compressibility, $C_w = 3.0 \times 10^{-6}$ psi^{-1}

Rock compressibility, $C_r = 4 \times 10^{-6}$ psi^{-1}

The fluid properties were specified by the following empirical equations:

$$\beta_o = 1.03 + 7.1 \times 10^{-5}P + 5.7 \times 10^{-8}P^2 \qquad P \leq P_b$$

$$\beta_o = \beta_{o_b} e^{-C_o(P - P_b)} \qquad P > P_b$$

$$\beta_w = 1.002 - 3 \times 10^{-6}P$$

$$\beta_g = 1./(-19.937 + 9.126 \times 10^{-2}P - 2.1086 \times 10^{-6}P^2$$

$$R_s = 24.0 + .253\ P \quad \text{ft}^3/\text{bbl} \qquad P \leq P_b$$

$$R_s = R_{s_b} \quad \text{ft}^3/\text{bbl} \qquad P > P_b$$

$$\mu_o = 2.239 - 7.16 \times 10^{-4}P + 7.7 \times 10^{-8}P^2 \quad \text{cp} \qquad P \leq P_b$$

$$\mu_o = \mu_{o_b} + 5 \times 10^{-5}(P - P_b) \quad \text{cp} \qquad P > P_b$$

$$\mu_w = .6246 \quad \text{cp}$$

$$\mu_g = 9 \times 10^{-3} + 5 \times 10^{-6}P \quad \text{cp}$$

$$\rho_o = 53.03 - .00487P - 6.3 \times 10^{-7}P^2 \quad \text{lb/ft}^3 \qquad P \leq P_b$$

$$\rho_o = \rho_{o_b} e^{-C_o(P - P_b)} \quad \text{lb/ft}^3 \qquad P > P_b$$

$$\rho_g = 2.932 \times 10^{-3}P \quad \text{lb/ft}^3$$

$$\rho_w = 62.275 + 1.875 \times 10^{-4}P \quad \text{lb/ft}^3$$

Relative Permeability Curve Shown in Figure 3A.

Capillary Pressure Curve shown in Figure 4A.

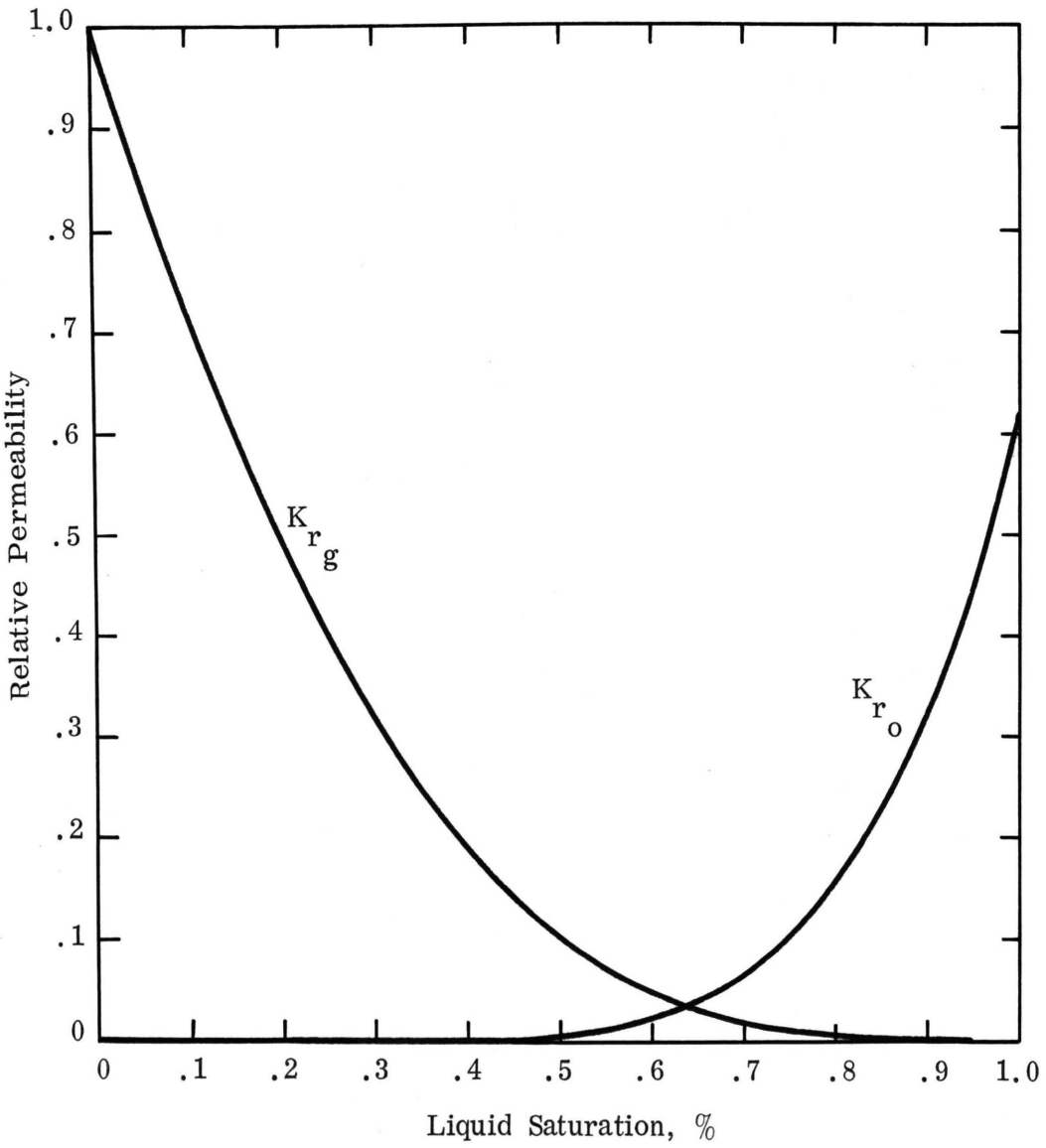

Figure 3A. Gas-Oil Relative Permeability Data

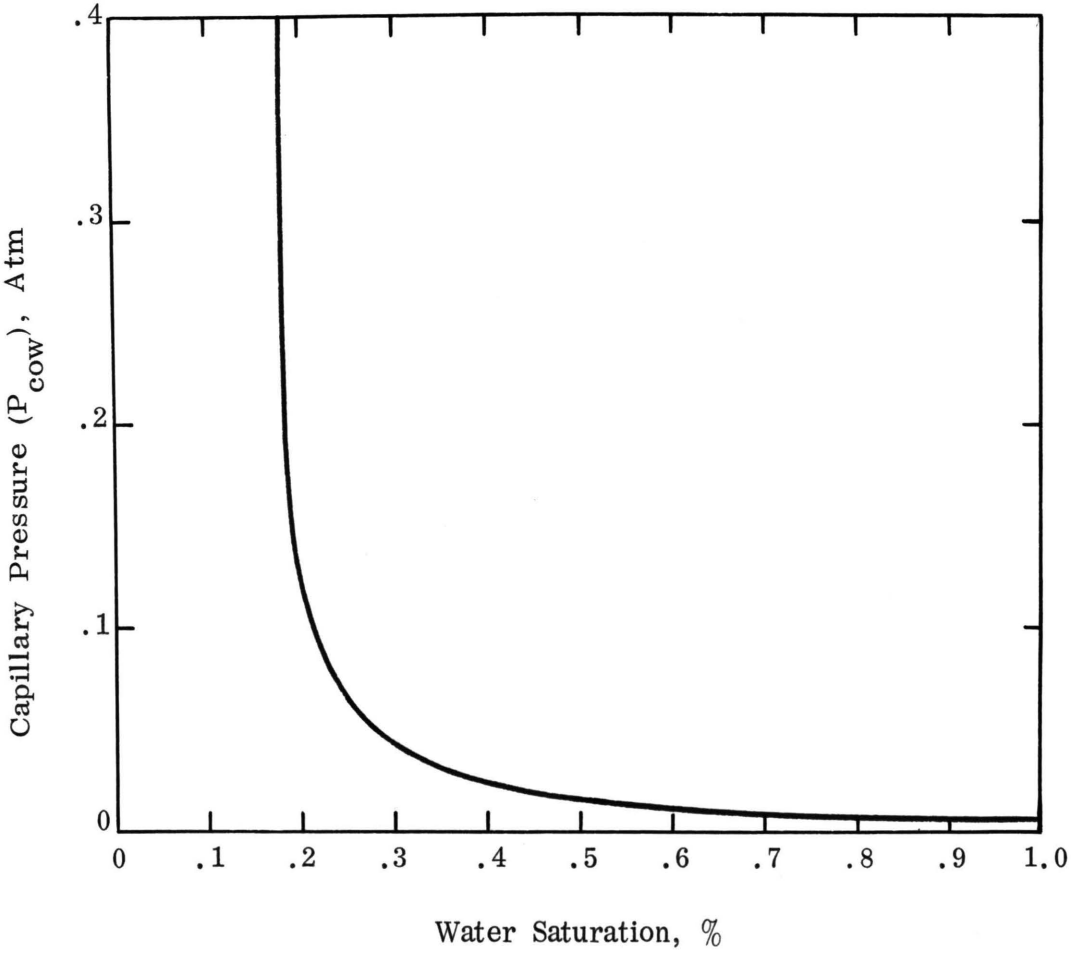

Figure 4A. Capillary Pressure Curve

APPENDIX F

FLOW CHART FOR SIMULATION MODELS

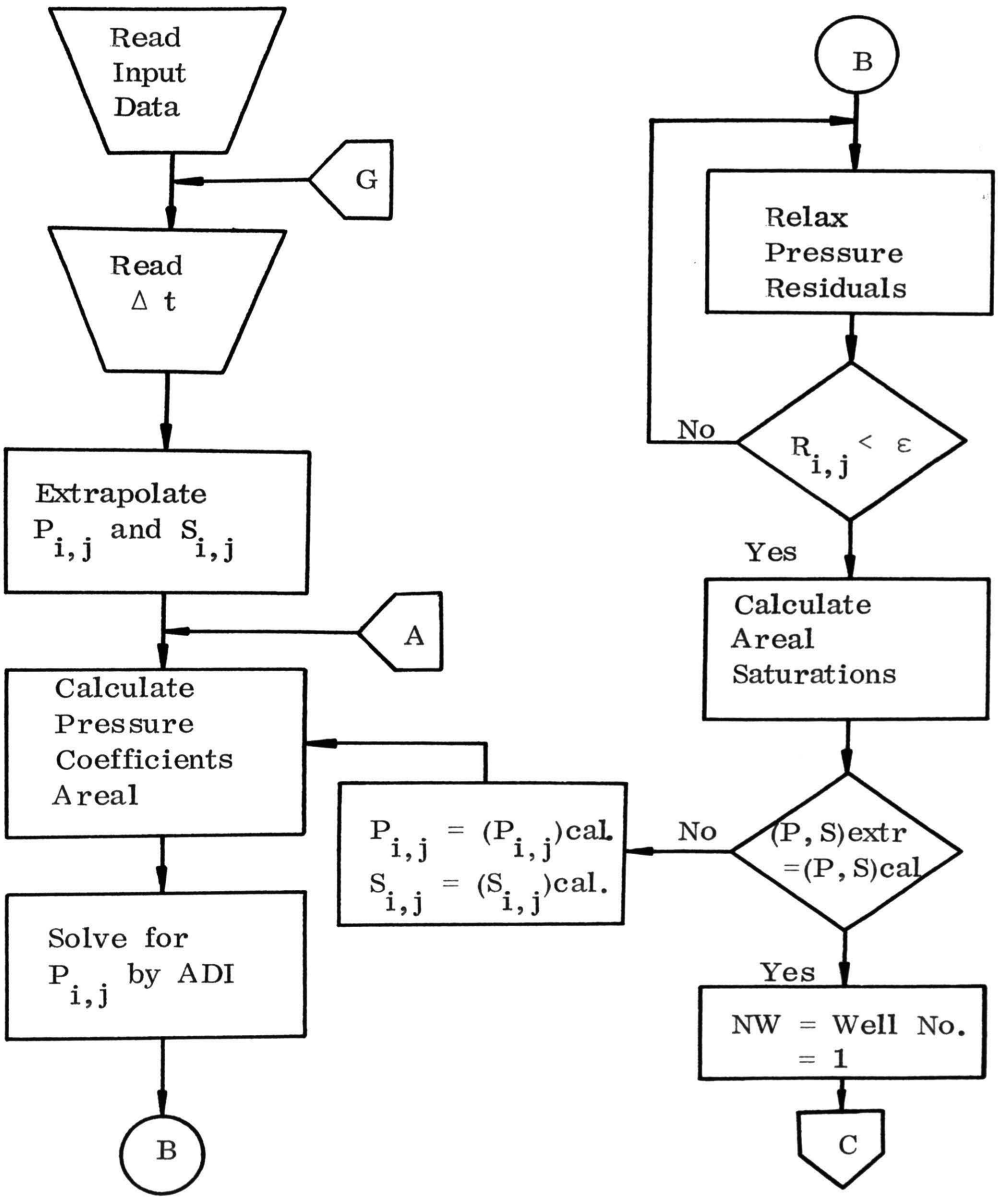

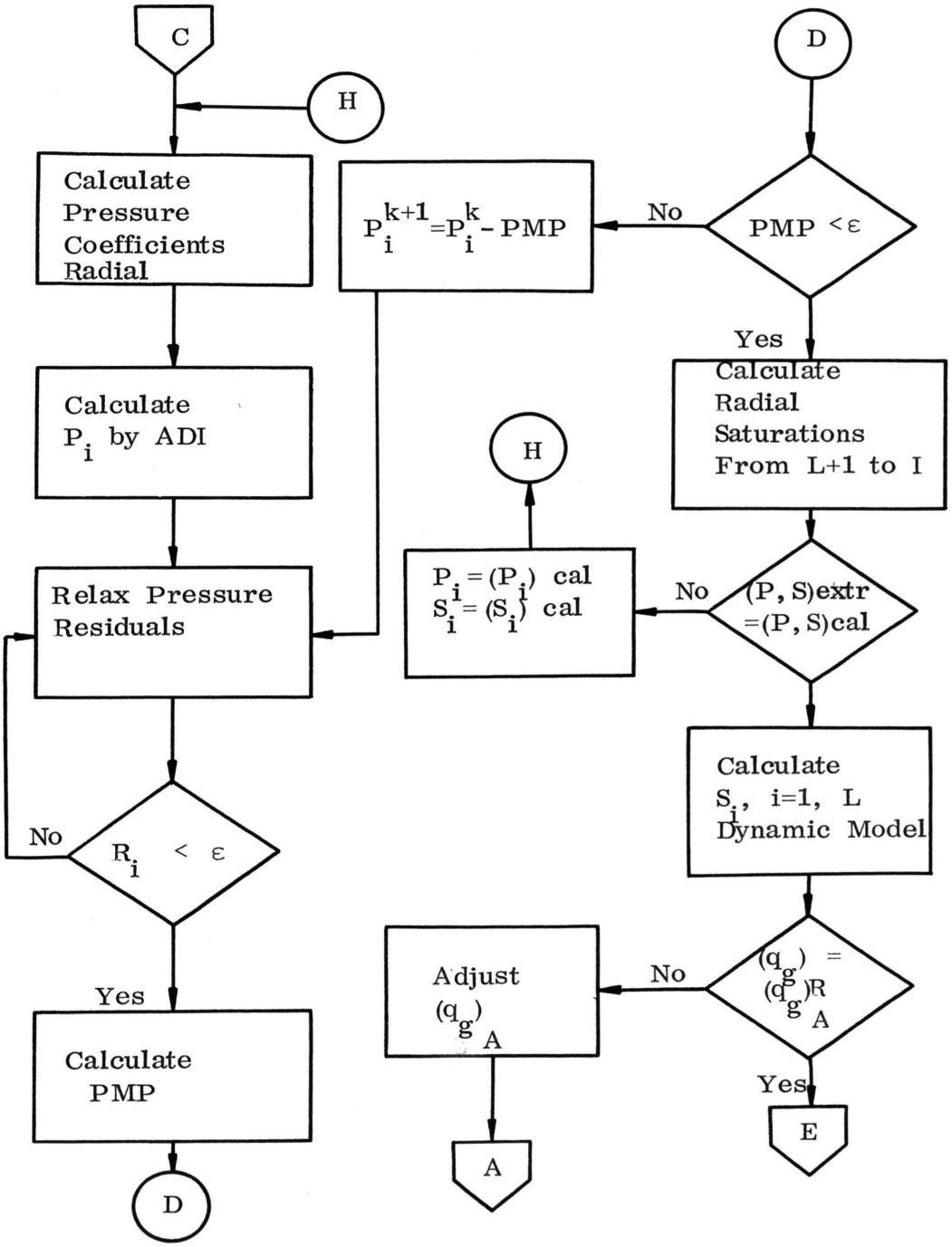
C
H
Calculate Pressure Coefficients Radial
Calculate P_i by ADI
Relax Pressure Residuals
No
$R_i < \varepsilon$
Yes
Calculate PMP
D
$P_i^{k+1} = P_i^k - PMP$
No
PMP $< \varepsilon$
Yes
Calculate Radial Saturations From L+1 to I
H
$P_i = (P_i)$ cal
$S_i = (S_i)$ cal
No
(P, S)extr = (P, S)cal
Calculate S_i, i=1, L Dynamic Model
Adjust $(q_g)_A$
No
$(q_g) = (q_g)_{RA}$
Yes
E
A

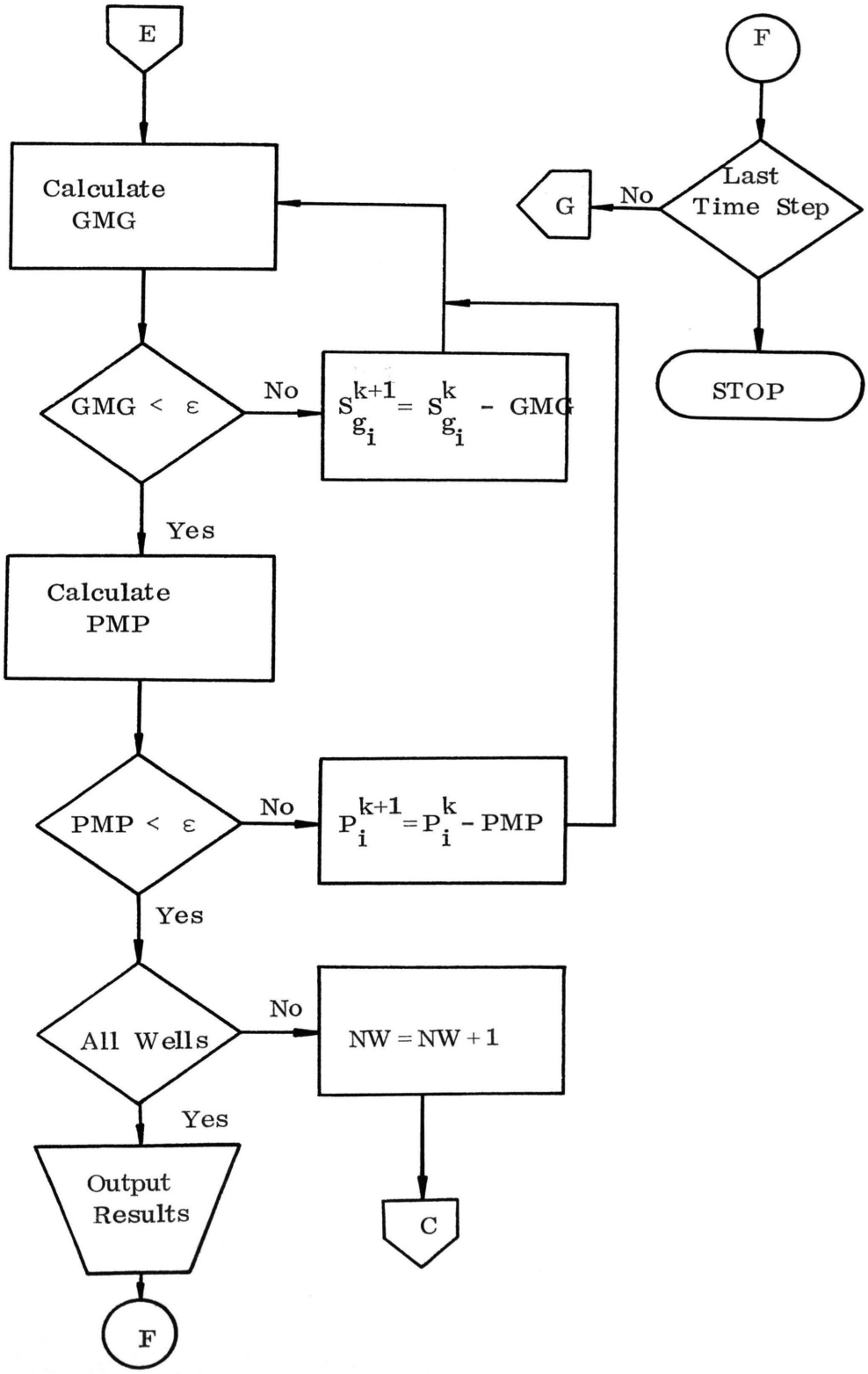
E
Calculate GMG
GMG < ε
No
$S_{g_i}^{k+1} = S_{g_i}^{k} - GMG$
Yes
Calculate PMP
PMP < ε
No
$P_i^{k+1} = P_i^{k} - PMP$
Yes
All Wells
No
NW = NW + 1
Yes
Output Results
F
C
F
Last Time Step
No
G
STOP